

**Nonequilibrium effects on the electron-phonon coupling constant in metals**Wuli Miao and Moran Wang <sup>\*</sup>*Key Laboratory for Thermal Science and Power Engineering of Ministry of Education,  
Department of Engineering Mechanics and CNMM, Tsinghua University, Beijing 100084, China* (Received 12 August 2020; revised 14 January 2021; accepted 4 February 2021; published 10 March 2021)

Understanding of the energy exchange between electrons and phonons in metals is important for micro- and nanomanufacturing and system design. The electron-phonon (*e-ph*) coupling constant describes such exchange strength, yet its variation remains still unclear at micro- and nanoscale where the nonequilibrium effects are significant. In this work, an *e-ph* coupling model is proposed by transforming the full scattering terms into relaxation time approximation forms in the coupled electron and phonon Boltzmann transport equations. Consequently, the nonequilibrium effects are included in the calculation of the *e-ph* coupling constant. The coupling model is verified by modeling the ultrafast dynamics in femtosecond pump-probe experiments on a metal surface, which shows consistent results with the full integral treatment of scattering terms. The *e-ph* coupling constant is strongly reduced due to both the temporal nonequilibrium between different phonon branches and the spatial nonequilibrium of electrons in confined space. The present work will promote not only a fundamental understanding of the *e-ph* coupling constant but also the theoretical description of coupled electron and phonon transport at micro- and nanoscale.

DOI: [10.1103/PhysRevB.103.125412](https://doi.org/10.1103/PhysRevB.103.125412)**I. INTRODUCTION**

Excitation of a metal by a femtosecond pulse laser involves a very complex process including electron-photon, electron-electron, electron-phonon, and phonon-phonon interactions [1,2]. In spite of its complexity, the preassumption of thermal equilibrium for electron and phonon subsystems is usually adopted, and electrons will exchange energy with phonons through electron-phonon (*e-ph*) scattering [3,4]. However, extensive experimental and theoretical studies have demonstrated the failure of the thermal equilibrium assumption due to both the nonthermalized electrons and the nonequilibrium between different phonon polarizations [5–12]. In addition, when the characteristic length of metals shrinks to nanoscale in micro- and nanoelectronics, the spatial nonequilibrium effect arising from size effect becomes significant [13,14]. These nonequilibrium effects will further influence the energy exchange between electrons and phonons.

In order to describe the strength of energy exchange in metals, the *e-ph* coupling constant defined as energy transfer rate per unit volume and per temperature difference between electrons and phonons is quantitatively introduced [15]. In 1957, Kaganov *et al.* studied the energy transfer through *e-ph* coupling firstly based on the Boltzmann transport theory and formulated an expression of the *e-ph* coupling constant. This expression connected the *e-ph* coupling constant to an empirical electron relaxation time, which was based on both the free electron gas model and thermal equilibrium for electron and phonon subsystems, respectively [16]. Nearly 30 years later, Allen insightfully related the coupling function

to the Eliashberg function in superconductivity, and then derived the corresponding theoretic formula of the *e-ph* coupling constant [17]. Later on, Allen's formula was validated by the femtosecond pulse laser experiments [18] and became a basic principle for most metals. However, the key assumption behind Allen's derivation was that both electrons and phonons were in thermal quasiequilibrium corresponding to their respective temperatures, which might be not valid at micro- and nanoscale [13,14].

Generally, the nonequilibrium effects are significant when the characteristic length of the system is comparable to the mean free path of heat carriers or the characteristic time of the process is comparable to the relaxation time. As a result, the transport properties such as thermal conductivity and electronic conductivity decrease notably from the standard bulk values [19,20]. In terms of the *e-ph* coupling constant, the results are not clear for thin films and nanoparticles in the literature by the different researchers using the femtosecond pump-probe experiments [21–28]. It remains inconclusive how the *e-ph* coupling constant varies when the characteristic length of metals reduces to nanoscale size. In ultrafast dynamics irradiated by a femtosecond pulse laser, nonthermalized electrons exist due to the finite electron-electron relaxation time [5–8,12]. This means that electrons have transferred energy to phonons before the electron subsystem reaches thermal equilibrium. An experiment in a pulse-heated metal showed that nonthermalized electrons make the *e-ph* energy relaxation process slower [7]. The theoretical analysis also showed that the *e-ph* coupling rate is weakened comparing to the thermalized limit at low excitation intensities [2,29]. Moreover, the coupling strength between electrons and different phonon branches is often different and thus the nonequilibrium between different phonon polarizations

<sup>\*</sup>mrwang@tsinghua.edu.cn

occurs [10,11]. However, it remains to investigate how the  $e$ - $ph$  coupling constant is influenced by this temporal nonequilibrium effect between different phonon branches. Therefore, this work aims to reveal the variation of the  $e$ - $ph$  coupling constant in metals at micro- and nanoscale when the spatial or temporal nonequilibrium effects are significant.

Current calculations of the  $e$ - $ph$  coupling constant are generally based on the semiclassical  $e$ - $ph$  scattering term in the Boltzmann transport equation which includes an  $e$ - $ph$  scattering matrix element representing alterations of electron states by absorbing or emitting a phonon [30]. The prevailing method is to solve the  $e$ - $ph$  scattering matrix element using *ab initio* calculation and thus the  $e$ - $ph$  coupling constant is computed by summing the energy change in the  $e$ - $ph$  scattering process [31–33]. This commonly used method is also based on the assumption of equilibrium for electron and phonon subsystems, respectively. In contrast, the direct solution of the coupled electron and phonon Boltzmann transport equations (BTEs) provides an alternative choice. Based on the evolution of distribution functions, the nonequilibrium effects can be intrinsically considered. However, the challenge of the coupled electron and phonon BTEs lies in the treatment of the scattering term due to its integral form and coupling between electron and phonon distribution functions, which makes the direct solution very difficult [2,9,29,34]. In addition to the linear-response assumption [9], the integral form of scattering terms is solvable as done by Rethfeld *et al.* [2] and Ono [34] when the drift term is neglected. Yet, with this treatment, it is hard to consider the drift term simultaneously which is necessary for the transport issues. In addition, there are also some macroscopic models to capture the coupled electron and phonon transport, including the two-temperature model (TTM) and the multitemperature model (MTM) with the  $e$ - $ph$  coupling constant as an input parameter [10,15,35–37]. Therefore, the other aim of this study is to propose a feasible treatment of the scattering term in the coupled electron and phonon BTEs. For solution of BTEs, two categories of numerical schemes are currently available, including a stochastic method such as the Monte Carlo (MC) scheme [38,39] and a deterministic method such as the discrete-ordinate method (DOM) [40,41]. The treatment of  $e$ - $ph$  coupling in MC schemes is still challenging so that we choose the DOM scheme first.

The “nonequilibrium” may have two kinds of meaning: (i) the “overall” nonequilibrium between electrons and phonons as their temperatures are different, and (ii) the “local” nonequilibrium as either electrons or phonons are not equilibrium in their own group. When talking about the  $e$ - $ph$  coupling constant, the “overall” nonequilibrium is default.

Therefore, in contrast, the present work focuses on the “local” nonequilibrium and studies the effects of this local nonequilibrium on the  $e$ - $ph$  coupling constant. The remainder of this article is organized as follows. In Sec. II, the theoretical derivation of the scattering model for the coupled electron and phonon BTEs is provided and the computational scheme for numerical solution is presented. The proposed coupling model is verified by modeling the ultrafast dynamics process in femtosecond pump-probe experiments. The variation of the  $e$ - $ph$  coupling constant is studied in Sec. III when nonequilibrium between different phonon branches or nonequilibrium of electrons exists. The concluding remarks are finally made in Sec. IV.

## II. THEORETICAL MODEL AND NUMERICAL METHOD

### A. Coupled electron and phonon BTEs under relaxation time approximation

The coupled electron and phonon BTEs without magnetic field are expressed as [42]

$$\frac{\partial f_{\mathbf{k}}}{\partial t} + \mathbf{v}_e \cdot \nabla_{\mathbf{r}} f_{\mathbf{k}} - \frac{e\mathbf{E}}{\hbar} \cdot \nabla_{\mathbf{k}} f_{\mathbf{k}} = \Omega_{e-ph}, \quad (1)$$

$$\frac{\partial n_{\mathbf{Q},p}}{\partial t} + \mathbf{v}_{ph,p} \cdot \nabla_{\mathbf{r}} n_{\mathbf{Q},p} = \Omega_{ph-e} + \Omega_{ph-ph}, \quad (2)$$

where  $f_{\mathbf{k}} \equiv f(\mathbf{r}, \mathbf{k}, t)$  is the electron distribution function denoting the electron occupation number around the wave vector  $\mathbf{k}$  and the spatial position  $\mathbf{r}$  at the moment  $t$  and  $n_{\mathbf{Q},p} \equiv n(\mathbf{Q}, p, \mathbf{r}, t)$  is the phonon distribution function with  $p$  the phonon polarizations and  $\mathbf{Q}$  the phonon wave vector.  $\mathbf{v}_e$  is the electron drift velocity with  $\mathbf{v}_{ph,p}$  the phonon group velocity of different polarizations.  $\hbar$  is the reduced Planck constant and  $\mathbf{E}$  is the effective electric field with  $e$  the element charge. In the scattering process, the  $e$ - $ph$  collision dominates for the alteration of electron distribution function, which is represented by  $\Omega_{e-ph}$ . Under low-fluence excitation and perturbation, the electron-electron interaction is very weak due to the greatly restricted scattering phase space by the Pauli exclusion principle [7,8]. Considering also the screened effect, the contribution from this electron-electron interaction is neglected as a first step [20,42].  $\Omega_{ph-e}$  and  $\Omega_{ph-ph}$  denote the alteration of the phonon distribution function by the phonon-electron ( $ph$ - $e$ ) scattering and phonon-phonon ( $ph$ - $ph$ ) scattering, respectively. The imperfection scattering is not considered as a first step, which can be incorporated in a straightforward way in the near future. Based on Fermi’s golden rule, the integral forms of  $\Omega_{e-ph}$  and  $\Omega_{ph-e}$  are formulated as

$$\begin{aligned} \Omega_{e-ph} = & -\frac{2\pi}{\hbar} \sum_{\mathbf{Q},p} |g(\mathbf{k}', \mathbf{k}, p)|^2 \{ f_{\mathbf{k}}(1 - f_{\mathbf{k}'}) [(n_{\mathbf{Q},p} + 1)\delta(\varepsilon_{\mathbf{k}} - \varepsilon_{\mathbf{k}'} - \hbar\omega_{\mathbf{Q},p}) + n_{\mathbf{Q},p}\delta(\varepsilon_{\mathbf{k}} - \varepsilon_{\mathbf{k}'} + \hbar\omega_{\mathbf{Q},p})] \\ & - (1 - f_{\mathbf{k}})f_{\mathbf{k}'} [(n_{\mathbf{Q},p} + 1)\delta(\varepsilon_{\mathbf{k}} - \varepsilon_{\mathbf{k}'} + \hbar\omega_{\mathbf{Q},p}) + n_{\mathbf{Q},p}\delta(\varepsilon_{\mathbf{k}} - \varepsilon_{\mathbf{k}'} - \hbar\omega_{\mathbf{Q},p})] \}, \quad (3) \end{aligned}$$

$$\Omega_{ph-e} = -\frac{2\pi}{\hbar} \sum_{\mathbf{k}} |g(\mathbf{k}', \mathbf{k}, p)|^2 f_{\mathbf{k}}(1 - f_{\mathbf{k}'}) [n_{\mathbf{Q},p}\delta(\varepsilon_{\mathbf{k}} - \varepsilon_{\mathbf{k}'} + \hbar\omega_{\mathbf{Q},p}) - (n_{\mathbf{Q},p} + 1)\delta(\varepsilon_{\mathbf{k}} - \varepsilon_{\mathbf{k}'} - \hbar\omega_{\mathbf{Q},p})], \quad (4)$$

where  $g(\mathbf{k}', \mathbf{k}, p)$  is the  $e$ - $ph$  scattering matrix element with its square representing the probability of electron transition from the state  $\mathbf{k}$  with energy  $\varepsilon_{\mathbf{k}}$  to the state  $\mathbf{k}'$  with energy  $\varepsilon_{\mathbf{k}'}$  by absorbing or emitting a phonon with frequency  $\omega_{\mathbf{Q},p}$  [19,42]. The summation of the electron wave vector state includes the spin degeneracy. In particular, the electron distribution function and phonon distribution function are strongly coupled with each other through the collision terms. In addition, the BTEs are integro-differential equations, which makes the direct solution very challenging.

Within the linear-response regime, the electron and phonon distribution function can be written as  $f_{\mathbf{k}} = f_{\mathbf{k}}^{eq}(\tilde{T}_e) + \Delta f_{\mathbf{k}}$ ,  $n_{\mathbf{Q},p} = n_{\mathbf{Q},p}^{eq}(\tilde{T}_{ph}) + \Delta n_{\mathbf{Q},p}$ , respectively, with the deviation part to be a small quantity  $\Delta f_{\mathbf{k}} \ll f_{\mathbf{k}}^{eq}(\tilde{T}_e)$ ,  $\Delta n_{\mathbf{Q},p} \ll n_{\mathbf{Q},p}^{eq}(\tilde{T}_{ph})$  away from the equilibrium state  $f_{\mathbf{k}}^{eq}(\tilde{T}_e)$ ,  $n_{\mathbf{Q},p}^{eq}(\tilde{T}_{ph})$  at the pseudotemperatures  $\tilde{T}_e$ ,  $\tilde{T}_{ph}$ , respectively. In this way, the  $e$ - $ph$  scattering term in Eq. (3) and the  $ph$ - $e$  scattering term in Eq. (4) are reformulated into

$$\begin{aligned} \Omega_{e-ph} = & -\frac{2\pi}{\hbar} \sum_{\mathbf{Q},p} |g(\mathbf{k}', \mathbf{k}, p)|^2 \left\{ [f_{\mathbf{k}}^{eq}(\tilde{T}_e) - f_{\mathbf{k}'}^{eq}(\tilde{T}_e)](n_{\mathbf{Q},p} - n_{\mathbf{Q},p}^{eq}(\tilde{T}_e)) + \Delta f_{\mathbf{k}}(n_{\mathbf{Q},p}^{eq}(\tilde{T}_{ph}) + 1 - f_{\mathbf{k}'}^{eq}(\tilde{T}_e)) \right. \\ & - \Delta f_{\mathbf{k}'}(n_{\mathbf{Q},p}^{eq}(\tilde{T}_{ph}) + f_{\mathbf{k}}^{eq}(\tilde{T}_e))] \delta(\varepsilon_{\mathbf{k}} - \varepsilon_{\mathbf{k}'} - \hbar\omega_{\mathbf{Q},p}) \\ & + [(f_{\mathbf{k}}^{eq}(\tilde{T}_e) - f_{\mathbf{k}'}^{eq}(\tilde{T}_e))(n_{\mathbf{Q},p} - n_{\mathbf{Q},p}^{eq}(\tilde{T}_e)) + \Delta f_{\mathbf{k}}(n_{\mathbf{Q},p}^{eq}(\tilde{T}_{ph}) + f_{\mathbf{k}}^{eq}(\tilde{T}_e)) \\ & \left. - \Delta f_{\mathbf{k}'}(n_{\mathbf{Q},p}^{eq}(\tilde{T}_{ph}) + 1 - f_{\mathbf{k}}^{eq}(\tilde{T}_e))] \delta(\varepsilon_{\mathbf{k}} - \varepsilon_{\mathbf{k}'} + \hbar\omega_{\mathbf{Q},p}) \right\}, \quad (5) \end{aligned}$$

$$\begin{aligned} \Omega_{ph-e} = & -\frac{2\pi}{\hbar} \sum_{\mathbf{k}} |g(\mathbf{k}', \mathbf{k}, p)|^2 \left\{ [f_{\mathbf{k}}^{eq}(\tilde{T}_e) - f_{\mathbf{k}'}^{eq}(\tilde{T}_e)] [n_{\mathbf{Q},p} - n_{\mathbf{Q},p}^{eq}(\tilde{T}_e)] + \Delta f_{\mathbf{k}} [n_{\mathbf{Q},p}^{eq}(\tilde{T}_{ph}) + f_{\mathbf{k}'}^{eq}(\tilde{T}_e)] \right. \\ & \left. - \Delta f_{\mathbf{k}'} [n_{\mathbf{Q},p}^{eq}(\tilde{T}_{ph}) + 1 - f_{\mathbf{k}}^{eq}(\tilde{T}_e)] \right\} \delta(\varepsilon_{\mathbf{k}} - \varepsilon_{\mathbf{k}'} + \hbar\omega_{\mathbf{Q},p}). \quad (6) \end{aligned}$$

Generally, the pseudotemperature of electrons,  $\tilde{T}_e$ , is different from that of phonons,  $\tilde{T}_{ph}$ , such that the expression  $n_{\mathbf{Q},p} - n_{\mathbf{Q},p}^{eq}(\tilde{T}_e)$  is formulated with  $n_{\mathbf{Q},p}^{eq}(\tilde{T}_e)$  at the electron pseudotemperature. This expression contains the nonequilibrium phonon part  $\Delta n_{\mathbf{Q},p}$  and the difference between the electron and phonon pseudotemperatures  $n_{\mathbf{Q},p}^{eq}(\tilde{T}_{ph}) - n_{\mathbf{Q},p}^{eq}(\tilde{T}_e)$ .

The nonequilibrium phonon in the electron scattering term in Eq. (5) is called phonon drag [43]. Correspondingly, the nonequilibrium electron in the phonon scattering term as shown by  $\Delta f_{\mathbf{k}}$  and  $\Delta f_{\mathbf{k}'}$  in Eq. (6) is called electron drag. These are mutual effects which fully couple the electron and phonon BTEs [44]. Nevertheless, the drag effects play a non-negligible role at a low temperature as the  $ph$ - $ph$  scatterings are greatly weakened and the phonons cannot get back to the local equilibrium quickly. At the temperature scope concerned in the present work, the drag effects are neglected as the first step. In addition, when dealing with the  $e$ - $ph$  scattering term in Eq. (5), the remaining terms  $n_{\mathbf{Q},p}^{eq}(\tilde{T}_{ph}) - n_{\mathbf{Q},p}^{eq}(\tilde{T}_e)$  implicitly contained in  $n_{\mathbf{Q},p} - n_{\mathbf{Q},p}^{eq}(\tilde{T}_e)$  are almost canceled with each other through the first-order Taylor expansion of the term  $f_{\mathbf{k}}^{eq}(\tilde{T}_e) - f_{\mathbf{k}'}^{eq}(\tilde{T}_e)$ . In other words, the terms  $n_{\mathbf{Q},p} - n_{\mathbf{Q},p}^{eq}(\tilde{T}_e)$  in the electron scattering term are negligible due to the inappreciable drag effect at the evaluated temperature and the nearly canceling summation of absorption and emission processes. Furthermore, under an isotropic scattering picture, the nonequilibrium  $\Delta f_{\mathbf{k}'}$  of other electron states in Eq. (5) vanishes by integration [45]. Therefore, the  $e$ - $ph$  scattering term in Eq. (5) and the  $ph$ - $e$  scattering term in Eq. (6) are simplified into the form of relaxation time approximation:

$$\begin{aligned} \Omega_{e-ph} = & -\frac{2\pi}{\hbar} \sum_{\mathbf{Q},p} |g(\mathbf{k}', \mathbf{k}, p)|^2 \left\{ \Delta f_{\mathbf{k}} [n_{\mathbf{Q},p}^{eq}(\tilde{T}_{ph}) + 1 - f_{\mathbf{k}'}^{eq}(\tilde{T}_e)] \delta(\varepsilon_{\mathbf{k}} - \varepsilon_{\mathbf{k}'} - \hbar\omega_{\mathbf{Q},p}) \right. \\ & \left. + \Delta f_{\mathbf{k}} [n_{\mathbf{Q},p}^{eq}(\tilde{T}_{ph}) + f_{\mathbf{k}}^{eq}(\tilde{T}_e)] \delta(\varepsilon_{\mathbf{k}} - \varepsilon_{\mathbf{k}'} + \hbar\omega_{\mathbf{Q},p}) \right\} \\ = & -\frac{\Delta f_{\mathbf{k}}}{\tau_{\mathbf{k},e-ph}} = -\frac{f_{\mathbf{k}} - f_{\mathbf{k}}^{eq}(\tilde{T}_e)}{\tau_{\mathbf{k},e-ph}}, \quad (7) \end{aligned}$$

$$\Omega_{ph-e} = -\frac{2\pi}{\hbar} \sum_{\mathbf{k}} |g(\mathbf{k}', \mathbf{k}, p)|^2 [f_{\mathbf{k}}^{eq}(\tilde{T}_e) - f_{\mathbf{k}'}^{eq}(\tilde{T}_e)] [n_{\mathbf{Q},p} - n_{\mathbf{Q},p}^{eq}(\tilde{T}_e)] \delta(\varepsilon_{\mathbf{k}} - \varepsilon_{\mathbf{k}'} + \hbar\omega_{\mathbf{Q},p}) = -\frac{n_{\mathbf{Q},p} - n_{\mathbf{Q},p}^{eq}(\tilde{T}_e)}{\tau_{\mathbf{Q},p,ph-e}}, \quad (8)$$

with the  $e$ - $ph$  and  $ph$ - $e$  scattering relaxation times defined, respectively, as

$$\begin{aligned} \frac{1}{\tau_{\mathbf{k},e-ph}} = & \frac{2\pi}{\hbar} \sum_{\mathbf{Q},p} |g(\mathbf{k}', \mathbf{k}, p)|^2 \left\{ [n_{\mathbf{Q},p}^{eq}(\tilde{T}_{ph}) + 1 - f_{\mathbf{k}'}^{eq}(\tilde{T}_e)] \delta(\varepsilon_{\mathbf{k}} - \varepsilon_{\mathbf{k}'} - \hbar\omega_{\mathbf{Q},p}) \right. \\ & \left. + [n_{\mathbf{Q},p}^{eq}(\tilde{T}_{ph}) + f_{\mathbf{k}}^{eq}(\tilde{T}_e)] \delta(\varepsilon_{\mathbf{k}} - \varepsilon_{\mathbf{k}'} + \hbar\omega_{\mathbf{Q},p}) \right\}, \quad (9) \end{aligned}$$

$$\frac{1}{\tau_{\mathbf{Q},p,ph-e}} = \frac{2\pi}{\hbar} \sum_{\mathbf{k}} |g(\mathbf{k}', \mathbf{k}, p)|^2 [f_{\mathbf{k}}^{eq}(\tilde{T}_e) - f_{\mathbf{k}'}^{eq}(\tilde{T}_e)] \delta(\varepsilon_{\mathbf{k}} - \varepsilon_{\mathbf{k}'} + \hbar\omega_{\mathbf{Q},p}). \quad (10)$$

The assumption of isotropic electron-acoustic phonon scattering in metals is nearly valid at a temperature higher than the Debye temperature.

Subsequently, we adopt the relaxation time approximation for the three-phonon umklapp scattering process with the normal scattering and high-order phonon-phonon scattering negligible at the phonon temperature regime in the present work. Thus, the  $ph-ph$  scattering is formulated as

$$\Omega_{ph-ph} = -\frac{n_{\mathbf{Q},p} - n_{\mathbf{Q},p}^{eq}(\tilde{T}_{ph})}{\tau_{U,ph-ph}}, \quad (11)$$

with the umklapp scattering spectral relaxation time defined as [46]

$$\frac{1}{\tau_{U,ph-ph}(\omega, p, \tilde{T}_{ph})} = B_U \omega^2 \tilde{T}_{ph} \exp(-\Theta_p/3\tilde{T}_{ph}). \quad (12)$$

In Eq. (12),  $B_U = \frac{\hbar\gamma_p^2}{M\Theta_p v_{ph,p}^2}$  with the Grüneisen parameter  $\gamma_p$  and Debye temperature  $\Theta_p$  for different phonon polarizations,  $M$  being the average atomic mass.

The assumption of distinct pseudotemperatures for TA and LA phonons when dealing with the  $e-ph$  scattering term in Eq. (5) and the  $ph-ph$  scattering term in Eq. (11) seems to be more consistent with the present study of nonequilibrium. However, the identical pseudotemperature for TA and LA phonons is adopted due to the following two aspects: (i) The influence of phonon pseudotemperature on the  $e-ph$  scattering term is only reflected in the expression of relaxation time in Eq. (9), where the distinguishing treatment of TA and LA phonons has negligible impact; (ii)  $ph-ph$  scattering pushes TA and LA phonons toward equilibrium and thus one representative phonon pseudotemperature in  $ph-ph$  scattering term is usually introduced [47]. Therefore, we assume an overall phonon pseudotemperature in dealing with  $e-ph$  and  $ph-ph$  scattering terms as an initial step.

For thermal transport, the contribution from the built-in electric field is negligibly small in metals [20,48] and neglected as demonstrated in our previous work [38]. With also the assumption of isotropic band structure and dispersion relation, the relaxation times of  $e-ph$  scattering and  $ph-e$  scattering are averaged on the same energy state as

$$\frac{1}{\tau_{e-ph}(\varepsilon)} = \frac{1}{D_e(\varepsilon)} \sum_{\mathbf{k}} \frac{1}{\tau_{\mathbf{k},e-ph}} \delta(\varepsilon - \varepsilon_{\mathbf{k}}), \quad (13)$$

$$\frac{1}{\tau_{ph-e}(\omega, p)} = \frac{1}{D_{ph}(\omega, p)} \sum_{\mathbf{Q}} \frac{1}{\tau_{\mathbf{Q},p,ph-e}} \delta(\omega - \omega_{\mathbf{Q},p}). \quad (14)$$

In Eqs. (13) and (14),  $D_e(\varepsilon)$  and  $D_{ph}(\omega, p)$  are the density of states (DOS) for electrons including the spin degeneracy and for phonons at different polarizations, respectively. With the help of the property of the Dirac  $\delta$  function, the following coupling functions are introduced as [34]

$$C_{e-ph}(\varepsilon, \varepsilon', \omega, p) = \frac{1}{\hbar D_e(\varepsilon)} \sum_{\mathbf{k}, \mathbf{Q}} |g(\mathbf{k}', \mathbf{k}, p)|^2 \delta(\varepsilon - \varepsilon_{\mathbf{k}}) \delta(\varepsilon' - \varepsilon_{\mathbf{k}'}) \delta(\omega - \omega_{\mathbf{Q},p}), \quad (15)$$

$$C_{ph-e}(\varepsilon, \varepsilon', \omega, p) = \frac{1}{\hbar D_{ph}(\omega, p)} \sum_{\mathbf{k}, \mathbf{Q}} |g(\mathbf{k}', \mathbf{k}, p)|^2 \delta(\varepsilon - \varepsilon_{\mathbf{k}}) \delta(\varepsilon' - \varepsilon_{\mathbf{k}'}) \delta(\omega - \omega_{\mathbf{Q},p}), \quad (16)$$

with the equation  $C_{ph-e}(\varepsilon, \varepsilon', \omega, p) = \frac{D_e(\varepsilon)}{D_{ph}(\omega, p)} C_{e-ph}(\varepsilon, \varepsilon', \omega, p)$ . The coupling function in Eq. (15) can be determined by *ab initio* calculation, or related to the Eliashberg function when neglecting the energy dependence of electron states [17,34]. Thus the spectral relaxation times in Eqs. (13) and (14) are formulated, respectively, as

$$\begin{aligned} \frac{1}{\tau_{e-ph}(\varepsilon)} = 2\pi \sum_p \int \left\{ [n_{\omega}^{eq}(\tilde{T}_{ph}) + 1 - f_{\varepsilon-\hbar\omega}^{eq}(\tilde{T}_e)] C_{e-ph}(\varepsilon, \varepsilon - \hbar\omega, \omega, p) \right. \\ \left. + [n_{\omega}^{eq}(\tilde{T}_{ph}) + f_{\varepsilon+\hbar\omega}^{eq}(\tilde{T}_e)] C_{e-ph}(\varepsilon, \varepsilon + \hbar\omega, \omega, p) \right\} d\omega, \end{aligned} \quad (17)$$

$$\frac{1}{\tau_{ph-e}(\omega, p)} = 2\pi \int \frac{D_e(\varepsilon)}{D_{ph}(\omega, p)} [f_{\varepsilon}^{eq}(\tilde{T}_e) - f_{\varepsilon+\hbar\omega}^{eq}(\tilde{T}_e)] C_{e-ph}(\varepsilon, \varepsilon + \hbar\omega, \omega, p) d\varepsilon. \quad (18)$$

Eventually, the strongly coupled electron and phonon BTEs (1) and (2) are greatly simplified into the relaxation time approximation forms:

$$\frac{\partial f_{\mathbf{k}}}{\partial t} + \mathbf{v}_e \cdot \nabla_{\mathbf{r}} f_{\mathbf{k}} = -\frac{f_{\mathbf{k}} - f_{\mathbf{k}}^{eq}(\tilde{T}_e)}{\tau_{e-ph}(\varepsilon)}, \quad (19)$$

$$\frac{\partial n_{\mathbf{Q},p}}{\partial t} + \mathbf{v}_{ph,p} \cdot \nabla_{\mathbf{r}} n_{\mathbf{Q},p} = -\frac{n_{\mathbf{Q},p} - n_{\mathbf{Q},p}^{eq}(\tilde{T}_e)}{\tau_{ph-e}(\omega, p)} - \frac{n_{\mathbf{Q},p} - n_{\mathbf{Q},p}^{eq}(\tilde{T}_{ph})}{\tau_{U,ph-ph}}, \quad (20)$$

with the relaxation times given by Eqs. (12), (17), and (18), respectively. The local pseudoequilibrium distributions for electrons and phonons are the Fermi-Dirac distribution and the Bose-Einstein distribution, respectively [49]:

$$f_{\mathbf{k}}^{eq}(\tilde{T}_e) = \frac{1}{\exp[(\varepsilon_{\mathbf{k}} - \mu)/k_B \tilde{T}_e] + 1}, \quad (21)$$

$$n_{\mathbf{Q},p}^{eq}(\tilde{T}_{ph}) = \frac{1}{\exp(\hbar\omega_{\mathbf{Q},p}/k_B \tilde{T}_{ph}) - 1}, \quad (22)$$

where  $k_B$  is the Boltzmann constant. The chemical potential  $\mu$  is very close to Fermi energy  $\varepsilon_F$  at the concerned temperature lower than around 1% of the corresponding Fermi temperature in this work, so that  $\mu = \varepsilon_F$  is assumed for simplicity without losing accuracy [49]. The  $e$ - $ph$  scattering connects the energy transfer between electrons and phonons so that the electron and phonon BTEs (19) and (20) are not decoupled and the simultaneous solution is essential. If under the preassumption that phonons are sufficiently thermalized to be in equilibrium with electrons, the coupled equations are automatically degraded to the electron BTE for the electron thermal transport.

### B. Computational scheme

In metals, only electrons around the Fermi energy with a width about the thermal energy unit ( $k_B T$ ) will respond to thermal perturbation [42]. Thus, we propose to consider the electron distribution  $f_{\mathbf{k}}$  above the Fermi energy and  $1-f_{\mathbf{k}}$  below the Fermi energy in the numerical simulation of electron thermal transport, as clearly demonstrated in our previous work [38]. For a compact mathematical expression, we introduce the following distribution function for electron thermal transport:

$$g_{\mathbf{k}} = H(\mu - \varepsilon) + [1 - 2H(\mu - \varepsilon)]f_{\mathbf{k}}, \quad (23)$$

where  $H(\mu - \varepsilon)$  is the Heaviside step function. Thus, the electron BTE for thermal transport is reformulated as

$$\frac{\partial g_{\mathbf{k}}}{\partial t} + \mathbf{v}_e \cdot \nabla_{\mathbf{r}} g_{\mathbf{k}} = -\frac{g_{\mathbf{k}} - g_{\mathbf{k}}^{eq}(\tilde{T}_e)}{\tau_{e-ph}(\varepsilon)}, \quad (24)$$

with  $g_{\mathbf{k}}^{eq}(\tilde{T}_e) = \{\exp(|\varepsilon_{\mathbf{k}} - \mu|/k_B \tilde{T}_e) + 1\}^{-1}$ .

The local pseudotemperatures, which are not explicitly involved in the original collision terms, need to be determined in the current form of relaxation time approximation. In particular, whatever the form of scattering terms are, the intrinsic conservation laws should always be obeyed during the corresponding scattering processes such as the  $e$ - $ph$  and  $ph$ - $ph$  scatterings. Thus, in terms of thermal transport, the energy conservation during the  $e$ - $ph$  scattering and  $ph$ - $ph$  scattering processes is implemented to determine the electron and phonon pseudotemperatures, respectively, as

$$\sum_{\mathbf{Q},p} \hbar\omega_{\mathbf{Q},p} \left[ -\frac{n_{\mathbf{Q},p} - n_{\mathbf{Q},p}^{eq}(\tilde{T}_{ph})}{\tau_{U,ph-ph}} \right] = 0, \quad (25)$$

$$\sum_{\mathbf{k}} |\varepsilon_{\mathbf{k}} - \mu| \left[ -\frac{g_{\mathbf{k}} - g_{\mathbf{k}}^{eq}(\tilde{T}_e)}{\tau_{e-ph}(\varepsilon)} \right] + \sum_{\mathbf{Q},p} \hbar\omega_{\mathbf{Q},p} \left[ -\frac{n_{\mathbf{Q},p} - n_{\mathbf{Q},p}^{eq}(\tilde{T}_e)}{\tau_{ph-e}(\omega, p)} \right] = 0, \quad (26)$$

and the details are shown in Appendix A. Consequently, the electron and phonon transport equations (24) and (20) combined with Eqs. (25) and (26) are complete for the description of coupled electron and phonon thermal transport process. The calculation of the  $e$ - $ph$  coupling constant is thus formulated as

$$G = \frac{(\frac{\partial E}{\partial t})_{ph-e}}{\tilde{T}_e - \tilde{T}_{ph}} = \frac{\sum_{\mathbf{Q},p} \hbar\omega_{\mathbf{Q},p} \left( -\frac{n_{\mathbf{Q},p} - n_{\mathbf{Q},p}^{eq}(\tilde{T}_e)}{\tau_{ph-e}(\omega, p)} \right)}{\tilde{T}_e - \tilde{T}_{ph}}, \quad (27)$$

the contribution to which can be conveniently divided into different phonon branches. In particular, through the description of distribution functions and the construction of  $e$ - $ph$  scattering and  $ph$ - $ph$  scattering processes, the nonequilibrium effects are naturally included.

Furthermore, under the present isotropic assumption, the intensity forms are introduced by multiplying Eqs. (24) and (20) by  $v_e |\varepsilon - \mu| D_e(\varepsilon)/4\pi$  and  $v_{ph,p} \hbar\omega D_{ph}(\omega, p)/4\pi$ , respectively:

$$\frac{\partial I_{\varepsilon}}{\partial t} + \mathbf{v}_e \cdot \nabla_{\mathbf{r}} I_{\varepsilon} = -\frac{I_{\varepsilon} - I_{\varepsilon}^{eq}(\tilde{T}_e)}{\tau_{e-ph}(\varepsilon)}, \quad (28)$$

$$\begin{aligned} \frac{\partial \phi_{\omega,p}}{\partial t} + \mathbf{v}_{ph,p} \cdot \nabla_{\mathbf{r}} \phi_{\omega,p} \\ = -\frac{\phi_{\omega,p} - \phi_{\omega,p}^{eq}(\tilde{T}_e)}{\tau_{ph-e}(\omega, p)} - \frac{\phi_{\omega,p} - \phi_{\omega,p}^{eq}(\tilde{T}_{ph})}{\tau_{U,ph-ph}}. \end{aligned} \quad (29)$$

The physical meaning of electron (phonon) intensity is the flux of energy per unit area, per unit time, per unit solid angle along the direction of electron (phonon) propagation, and per unit energy (frequency) interval around  $\varepsilon$  ( $\omega$ ) [50]. The local pseudoequilibrium intensities are formulated, respectively, as  $I_{\varepsilon}^{eq}(\tilde{T}_e) = v_e |\varepsilon - \mu| g_{\varepsilon}^{eq}(\tilde{T}_e) D_e(\varepsilon)/4\pi$  and  $\phi_{\omega,p}^{eq}(\tilde{T}_{ph}) = v_{ph,p} \hbar\omega n_{\omega,p}^{eq}(\tilde{T}_{ph}) D_{ph}(\omega, p)/4\pi$ , where the pseudotemperature is computed by the inverse numerical integration of Eqs. (25) and (26) transformed into intensity forms as

$$\sum_p \iint_{4\pi} \left[ -\frac{\phi_{\omega,p} - \phi_{\omega,p}^{eq}(\tilde{T}_{ph})}{v_{ph,p} \tau_{U,ph-ph}} \right] d\Omega d\omega = 0, \quad (30)$$

$$\begin{aligned} \iint_{4\pi} \left[ -\frac{I_{\varepsilon} - I_{\varepsilon}^{eq}(\tilde{T}_e)}{v_e \tau_{e-ph}(\varepsilon)} \right] d\Omega d\varepsilon \\ + \sum_p \iint_{4\pi} \left[ -\frac{\phi_{\omega,p} - \phi_{\omega,p}^{eq}(\tilde{T}_e)}{v_{ph,p} \tau_{ph-e}(\omega, p)} \right] d\Omega d\omega = 0. \end{aligned} \quad (31)$$

The temperature dependence of the spectral relaxation times is considered in the numerical solution.

To sum up, we obtain the intensity forms of the coupled electron and phonon BTEs for numerical solution. Once the electron and phonon intensities are resolved, the  $e$ - $ph$  coupling constant  $G$  and the local electron and phonon energy density  $E_e(t, \mathbf{r})$ ,  $E_{ph}(t, \mathbf{r})$  with the respective local temperature  $T_e$  and  $T_{ph}$  are thus calculated:

$$G = \frac{(\frac{\partial E}{\partial t})_{ph-e}}{\tilde{T}_e - \tilde{T}_{ph}} = \frac{\sum_p \iint_{4\pi} \left[ -\frac{\phi_{\omega,p} - \phi_{\omega,p}^{eq}(\tilde{T}_e)}{v_{ph,p} \tau_{ph-e}(\omega, p)} \right] d\Omega d\omega}{\tilde{T}_e - \tilde{T}_{ph}}, \quad (32)$$

$$E_e(t, \mathbf{r}) = \iint_{4\pi} \frac{I_{\varepsilon}}{v_e} d\Omega d\varepsilon = \iint_{4\pi} \frac{I_{\varepsilon}^{eq}(T_e)}{v_e} d\Omega d\varepsilon, \quad (33)$$

$$\begin{aligned}
E_{ph}(t, \mathbf{r}) &= \sum_p \iint_{4\pi} \frac{\phi_{\omega,p}}{v_{ph,p}} d\Omega d\omega \\
&= \sum_p \iint_{4\pi} \frac{\phi_{\omega,p}^{eq}(T_{ph})}{v_{ph,p}} d\Omega d\omega. \quad (34)
\end{aligned}$$

The DOM scheme is adopted for the numerical solution, the development and validity of which have been demonstrated in our previous work [40,41]. Additionally, the Gauss-Legendre (GL) quadrature is adopted for the numerical integration over the electron energy, phonon frequency, and angular variables due to its high efficiency as shown in Appendix B.

### C. Model verification

The coupled electron and phonon BTEs in Secs. II A and II B will be verified by numerical modeling of the ultrafast dynamics process in femtosecond pump-probe experiments. A direct comparison with the experiment is difficult because the probed signal, such as the reflectance change of metal surface, includes the contribution from both electrons and phonons with the ratio to each other dependent on the probe laser and material. As the validation of the relaxation time approximation of the  $e$ - $ph$  coupling in the present model is the key point, we compare the present coupling model to the full integral treatment of scattering terms in Ono's model [34]. The widely used continuum models such as the two-temperature model (TTM) and the four-temperature model (FTM) are also included for comparison.

Neglecting the drift term is often adopted for simplicity when investigating the ultrafast dynamics in femtosecond pump-probe experiments since the characteristic timescale of coupling and energy transfer between electrons and phonons is very short [34]. The initial condition, electron Fermi window, phonon dispersion relation, and the expression of  $e$ - $ph$  coupling function in Eq. (15) for aluminum are all referred from Ono's model [34]. The Grüneisen parameters in the three-phonon umklapp scattering term for different phonon polarizations are adopted, respectively, as  $\gamma_{TA} = 2.21$ ,  $\gamma_{LA} = 2.21$  [31]. In the DOM scheme for numerical solution, the angular and spatial variables vanish in this case due to the negligible treatment of the drift term. The discretization of the electron energy and phonon spectrum is based on the abscissas of the GL quadrature that are applied with 96 and 80 points for electrons and phonons, respectively. The time step is set to be 1 fs.

The electron and phonon energy densities,  $E_e(t)$  and  $E_{ph}(t)$ , are calculated by Eqs. (33) and (34), respectively, without the spatial dependence. Based on this computation, the excess electron and phonon energy densities defined as  $E_e^* = E_e(t) - E_e(T_0)$ ,  $E_{ph}^* = E_{ph}(t) - E_{ph}(T_0)$ , respectively, with the reference temperature  $T_0 = 290$  K are shown in Fig. 1. The electron energy density decreases with time accompanied by the increase of phonon energy density due to the energy transfer between each other. Ono's work demonstrates that the energy relaxation in the continuum models with the quasiequilibrium treatment such as TTM and FTM is obviously faster than that in his BTE model [34]. Although the present result is

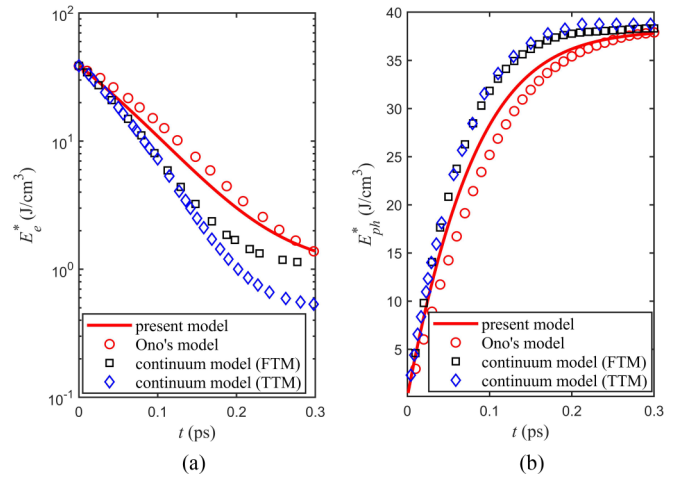


FIG. 1. Time-dependent excess electron and phonon energy density: (a) excess electron energy density; (b) excess phonon energy density; the solid line denotes the result of the present coupling model whereas hollow circles, squares, and diamonds are that of Ono's model, FTM, and TTM, respectively [34].

slightly faster than that of Ono's model due to the assumption of weak deviation from the equilibrium state, the agreement is generally very good in contrast to the TTM and FTM. For some femtosecond pump-probe experiments where electrons are highly excited to be thousands of Kelvin instantly, the higher-order nonequilibrium effects might be relevant and the integral treatment of the full scattering term is more preferable. Nevertheless, in most transport cases within the linear-response regime, the present treatment of  $e$ - $ph$  coupling by relaxation time approximation provides a more practical avenue. It represents a more accurate theoretical description compared to the continuum model whereas it is a simpler one compared to BTE with full scattering term. In summary, the comparison of the results by our relaxation time approximation model with that by Ono's model provides a solid validation of our  $e$ - $ph$  coupling model.

### III. RESULTS AND DISCUSSION

In this section, we will apply the validated  $e$ - $ph$  coupling model to study the  $e$ - $ph$  coupling constant for four kinds of metals including aluminum, copper, silver, and gold. The influences on the  $e$ - $ph$  coupling constant by the temporal nonequilibrium between different phonon branches and the spatial nonequilibrium of electrons are investigated in Secs. III A and III B, respectively.

The electron band structure is approximated as the free electron model and the electron Fermi window is adopted as  $[\varepsilon_F - 15k_B T, \varepsilon_F + 15k_B T]$  with  $T = 500$  K. The phonon dispersion relation along the  $[001]$  direction is used to represent the dispersion in the first Brillouin zone, and is fitted by an empirical power law expression:  $\omega(q) = B_{4,p}q^4 + B_{3,p}q^3 + B_{2,p}q^2 + B_{1,p}q$  with fitting parameters  $B_{1,p}$ ,  $B_{2,p}$ ,  $B_{3,p}$ , and  $B_{4,p}$ . This expression for different metals is referred from experimental data [51–54] or theoretic calculation [55] as summarized in Table I. The nondimensional parameter

TABLE I. Phonon dispersion relation along the [0 0 1] direction for different metals including aluminum, silver, copper, and gold at 300 K.

	TA branch (rad/s)	LA branch (rad/s)
Al	$6.750 \times 10^{12} q^4 - 3.204 \times 10^{13} q^3$ $+ 9.578 \times 10^{12} q^2 + 5.147 \times 10^{13} q$	$6.208 \times 10^{13} q^4 - 1.216 \times 10^{14} q^3$ $+ 2.226 \times 10^{13} q^2 + 9.825 \times 10^{13} q$
Ag	$8.1289 \times 10^{12} q^4 - 2.4607 \times 10^{13} q^3$ $+ 4.4373 \times 10^{12} q^2 + 3.3748 \times 10^{13} q$	$1.5349 \times 10^{13} q^4 - 3.8537 \times 10^{13} q^3$ $+ 0.7202 \times 10^{12} q^2 + 5.4066 \times 10^{13} q$
Cu	$1.0452 \times 10^{13} q^4 - 3.5385 \times 10^{13} q^3$ $+ 7.6611 \times 10^{12} q^2 + 4.9674 \times 10^{13} q$	$4.0666 \times 10^{12} q^4 - 2.643 \times 10^{13} q^3$ $- 6.351 \times 10^{12} q^2 + 7.4353 \times 10^{13} q$
Au	$1.1451 \times 10^{12} q^4 - 1.3922 \times 10^{13} q^3$ $+ 7.7833 \times 10^{12} q^2 + 2.2398 \times 10^{13} q$	$4.0651 \times 10^{12} q^4 - 8.6902 \times 10^{12} q^3$ $- 2.1783 \times 10^{13} q^2 + 5.5651 \times 10^{13} q$

is expressed as  $q = Q/Q_{\max}$  with  $Q$  the phonon wave vector along the [0 0 1] direction and  $Q_{\max} = 2\pi/a$ ,  $a$  being the cubic lattice constant. Transverse acoustic (TA) polarization and longitudinal acoustic (LA) polarization are included for calculation. The Grüneisen parameters for different phonon branches are chosen to be the same [31,33,56] as summarized in Table II. In addition, the  $e$ - $ph$  coupling function is related to the Eliashberg function and approximated as  $C_{e-ph}(\varepsilon, \varepsilon', \omega, p) \simeq \sqrt{\varepsilon_F/\varepsilon} \alpha^2 F(\omega, p)$  for the convenience of considering the deviation of electron energy from the Fermi level [34]. Furthermore, an empirical expression originally derived in the low-frequency limit is adopted for the Eliashberg function in the whole frequency spectrum:  $\alpha^2 F(\omega, p) = \lambda_p n(\omega/\omega_{\max,p})^n/2$  with  $n$  equal to 2 for a clean bulk crystal [57]. The mass enhancement parameter  $\lambda_p$  for different polarizations can be inversely determined as  $\lambda_p = 2 \int_0^{\omega_{\max,p}} \frac{\alpha^2 F(\omega,p)}{\omega} d\omega$  once the Eliashberg function is obtained [58]. As the overall mass enhancement parameter  $\lambda = 2\lambda_{TA} + \lambda_{LA}$  is usually given by *ab initio* theoretical calculation [31–33] or experimental measurement [58], the contribution from different phonon branches is often not given. Thus the ratio of different branches is referred from the empirical calculation for aluminum [34] and is approximated to be  $\lambda_{LA} : \lambda_{TA} \approx 2 : 1$  as given in Table II. This value is consistent with the theoretical analysis that the  $e$ - $ph$  coupling is dominated by LA phonons [10].

In order to validate the parameters adopted in our model, the electron thermal conductivity

$$\kappa_e = \int_{\text{Fermi window}} (\varepsilon - \varepsilon_F) \frac{df^{eq}}{dT} v_e^2 \tau_{e-ph}(\varepsilon) D_e(\varepsilon) d\varepsilon/3,$$

TABLE II. Summary of electron Fermi energy  $\varepsilon_F$ , cubic lattice constant  $a$ , overall mass enhancement parameter  $\lambda$  including the contribution from TA polarization  $\lambda_{TA}$  and LA porization  $\lambda_{LA}$ , and Grüneisen parameters  $\gamma_{TA}$ ,  $\gamma_{LA}$  for the TA, LA branches for different metals at 300 K.

	$\varepsilon_F$ (eV) [49]	$a$ (Å) [49]	$\lambda$	$\lambda_{TA}$	$\lambda_{LA}$	$\gamma_{TA}$	$\gamma_{LA}$
Al	11.63	4.05	0.45	0.12	0.21	2.21	2.21
Ag	5.48	4.09	0.12	0.03	0.06	2.31	2.31
Cu	7.00	3.61	0.18	0.045	0.09	1.94	1.94
Au	5.51	4.08	0.15	0.04	0.07	2.62	2.62

phonon thermal conductivity

$$\kappa_{ph} = \sum_p \int_0^{\omega_{\max,p}} \hbar\omega \frac{dn^{eq}}{dT} v_{ph,p}^2 (\tau_{ph-e}^{-1} + \tau_{ph-ph}^{-1})^{-1} \times D_{ph}(\omega, p) d\omega/3$$

based on the kinetic theory [42], and the  $e$ - $ph$  coupling constant  $G = 3\hbar \int_{\text{Fermi window}} (\varepsilon - \varepsilon_F) \frac{df^{eq}}{dT} D_e(\varepsilon) d\varepsilon \times \sum_p 2 \int_0^{\omega_{\max,p}} \frac{\alpha^2 F(\omega,p)}{\omega} \omega^2 d\omega / (\pi k_B T)$  based on Allen's formula [17] are, respectively, calculated for aluminum, silver, copper, and gold, as summarized in Table III. The overall thermal conductivity summing the contribution from electrons and phonons as  $\kappa = \kappa_e + \kappa_{ph}$  is also shown. We compare the results of the present calculation with those by *ab initio* calculation [31–33] and experimental measurements [49,58,59]. For the overall thermal conductivity of Al, there exists an appreciable difference between the experimental data and the present result, which may arise from the calculation of the Fermi velocity [60]. For the thermal conductivities of Al and Cu contributed by phonons, the results of the present work are a little lower than those by the *ab initio* method. It might be attributed to the power law approximation of the Eliashberg function in the whole spectrum, which may slightly overpredict the  $ph$ - $e$  scattering rate for the medium-high frequency. Thus, the corresponding phonon thermal conductivity of Al or Cu with a higher Debye temperature may be underestimated slightly. Generally, the  $e$ - $ph$  coupling constant and overall thermal conductivity calculated by the present work agree with the *ab initio* results and experimental data, which validates the input parameters adopted in our model.

### A. Temporal nonequilibrium effect on $e$ - $ph$ coupling constant

In this section, the  $e$ - $ph$  coupling constant in ultrafast dynamics is calculated. For simplicity, the drift term is neglected as a first step. The initial condition is set that electrons are assumed in equilibrium at 980 K with phonons undisturbed at room temperature (300 K). This choice of initial condition is to approach the condition in femtosecond pump-probe experiments as a first step. The time step for aluminum, silver, copper, and gold is adopted to be 2, 10, 2, and 8 fs, separately. The number of abscissas of the GL quadrature is chosen as 96 and 80 points for electron energy and phonon spectrum, respectively. Thus, the time-dependent  $e$ - $ph$  coupling constant

TABLE III. Summary of electron thermal conductivity  $\kappa_e$ , phonon thermal conductivity  $\kappa_{ph}$ , overall thermal conductivity  $\kappa$ , and  $e$ - $ph$  coupling constant  $G$  calculated by the present work in comparison with *ab initio* results [31–33] or experimental data [49,58,59] for different metals at 300 K.

		$\kappa_e$ (W/m/K)	$\kappa_{ph}$ (W/m/K)	$\kappa$ (W/m/K)	$G$ (W/m <sup>3</sup> /K)
Al	Present calculation	335.24	3.91	339.15	$3.62 \times 10^{17}$
	<i>Ab initio</i>	232.53 [33], 246 [31]	8.95 [33],5.8 [32], 6 [31]	241.49 [33], 252 [31]	$5.38 \times 10^{17}$ [31]
	Experiment	–	–	237 [49]	$2.45 \times 10^{17}$ [59]
Ag	Present calculation	404.94	4.94	409.88	$2.01 \times 10^{16}$
	<i>Ab initio</i>	450.86 [33], 370 [31]	5.69 [33], 5.2 [32], 4 [31]	456.55 [33], 374 [31]	$3.0 \times 10^{16}$ [31]
	Experiment	–	–	429 [49]	–
Cu	Present calculation	388.55	10.26	398.81	$7.25 \times 10^{16}$
	<i>Ab initio</i>	361.32 [33]	17.42 [33], 16.9 [32]	378.74 [33]	–
	Experiment	–	–	401 [49]	$\sim 1 \times 10^{17}$ [58]
Au	Present calculation	326.88	4.05	330.93	$1.92 \times 10^{16}$
	<i>Ab initio</i>	273.45 [33], 276 [31]	2.80 [33], 2.6 [32], 2 [31]	276.25 [33], 278 [31]	$2.2 \times 10^{16}$ [31]
	Experiment	–	–	317 [49]	$2.9 \times 10^{16}$ [59]

calculated by Eq. (32) and the electron and phonon temperature computed by the inverse integration of Eqs. (33) and (34) are shown in Fig. 2 for different metals. The energy transfer occurs between electrons and phonons, which is clearly shown by the decrease of electron temperature and increase of phonon temperature until the temperature difference between the two vanishes. The  $e$ - $ph$  coupling constant predicted by Allen's theory is constant within the temperature scope concerned in the present work, where the excitation of  $d$  band electrons is not necessarily considered. In comparison, the  $e$ - $ph$  coupling constant calculated by the present model remains nearly constant and a little lower than that predicted by Allen's theory at the initial stage, rapidly decreasing at some moment, and finally reducing to the value one order of magnitude smaller than that of Allen's theory. The temperature difference between electron and phonon is still appreciable (27.2, 5.6, 10.8, and 7.1 K for aluminum, silver, copper, and gold, separately) when the  $e$ - $ph$  coupling constant reduces to half of Allen's theoretical value. In addition, the occurrence instant of this rapid reduction is different for different metals.

For the further understanding of this reduction, the  $e$ - $ph$  coupling constant in Eq. (32) including the contribution of different phonon branches is correspondingly divided and shown in Fig. 3 for Ag. This reduction is almost attributed to the LA branch whereas the  $e$ - $ph$  coupling constant due to the TA branch remains nearly constant. The present trend is also applicable for other metals including aluminum, copper, and gold, and is not shown here to avoid repetition. The  $e$ - $ph$  coupling constant contributed by the LA branch even reduces to be negative, which means that LA phonons transfer energy to electrons. Such anomalous phenomena of energy backflow has also been demonstrated in Ono's model [34].

Furthermore, in order to investigate how the energy backflow occurs, the TA and LA phonon energy density change rates by the  $e$ - $ph$  scattering and  $ph$ - $ph$  scattering are defined as  $(\partial E_{ph,TA}/\partial t)_{ph-e}$ ,  $(\partial E_{ph,LA}/\partial t)_{ph-e}$ ,  $(\partial E_{ph,TA}/\partial t)_{ph-ph}$ , and  $(\partial E_{ph,LA}/\partial t)_{ph-ph}$ , separately. Considering the phonon BTE, the phonon energy density change rates are equal to the energy transfer during the corresponding  $e$ - $ph$  and  $ph$ - $ph$  scattering channels. Thus, the phonon energy density change rates are

calculated as

$$(\partial E_{ph,TA}/\partial t)_{ph-e} = \iint_{4\pi} \left[ -\frac{\phi_{\omega,TA} - \phi_{\omega,TA}^{eq}(\tilde{T}_e)}{v_{ph,TA} \tau_{ph-e}(\omega,TA)} \right] d\Omega d\omega,$$

$$(\partial E_{ph,LA}/\partial t)_{ph-e} = \iint_{4\pi} \left[ -\frac{\phi_{\omega,LA} - \phi_{\omega,LA}^{eq}(\tilde{T}_e)}{v_{ph,LA} \tau_{ph-e}(\omega,LA)} \right] d\Omega d\omega,$$

$$(\partial E_{ph,TA}/\partial t)_{ph-ph} = \iint_{4\pi} \left[ -\frac{\phi_{\omega,TA} - \phi_{\omega,TA}^{eq}(\tilde{T}_{ph})}{v_{ph,TA} \tau_{U,ph-ph}} \right] d\Omega d\omega,$$

and

$$(\partial E_{ph,LA}/\partial t)_{ph-ph} = \iint_{4\pi} \left[ -\frac{\phi_{\omega,LA} - \phi_{\omega,LA}^{eq}(\tilde{T}_{ph})}{v_{ph,LA} \tau_{U,ph-ph}} \right] d\Omega d\omega;$$

they are shown in Fig. 4(a).

Figure 4(b) shows the excess energy density of electrons and phonons at different polarizations with the reference temperature of 300 K. During the initial stage to 0.3 ps, the energy exchange by the  $e$ - $ph$  scattering dominates and the strength of the electron-LA-phonon ( $e$ -LA) scattering is stronger than that of the electron-TA-phonon ( $e$ -TA) scattering. It is clearly shown in Fig. 4(b) that the energy increase of LA phonons is much faster than that of TA phonons such that nonequilibrium occurs between different phonon branches. This nonequilibrium effect continually enlarges from 0.3 to 2 ps due to the continuous dominance of  $e$ - $ph$  scattering though  $ph$ - $ph$  scattering gradually works, pushing LA and TA phonons to be in equilibrium. Afterward, during the next 7 ps,  $ph$ - $ph$  scattering gradually dominates and thus the nonequilibrium between TA and LA phonons is weakened but still exists. Considering the continually decreasing amount of energy exchange by  $e$ - $ph$  scattering, the energy transfer from electrons to LA phonons rapidly decreases to be negative around 9 ps. In other words, energy backflow takes place, the clear signature of which is revealed in the inset of Fig. 4(a).

In general, the intrinsically different dispersion relation for TA and LA phonons and the different coupling strength for  $e$ -LA and  $e$ -TA scattering represented by the coupling function in Eq. (15) will induce nonequilibrium between different phonon polarizations. This will further make the  $ph$ - $ph$  scattering gradually work, pushing the equilibrium between TA and LA phonons. Considering these effects, the temporal

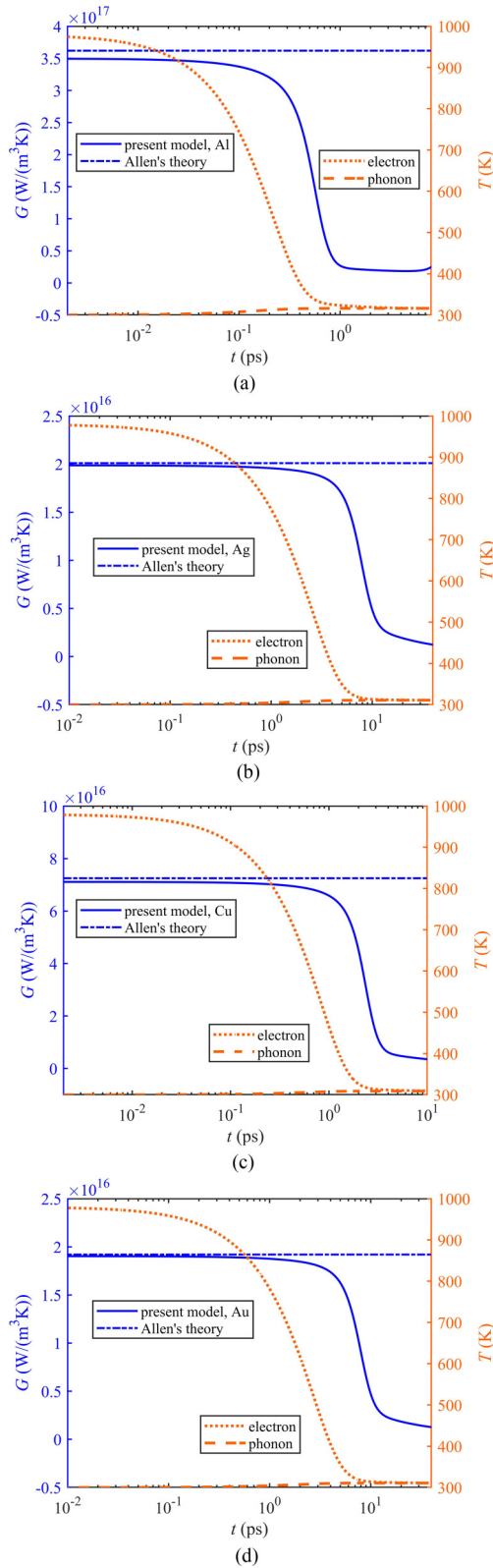


FIG. 2. Time-dependent  $e$ - $ph$  coupling constant and electron, phonon temperature in ultrafast dynamics: (a) for aluminum; (b) for silver; (c) for copper; (d) for gold. The solid blue line represents the  $e$ - $ph$  coupling constant calculated by the present model whereas the blue dash-dot line denotes that from Allen's theory [17]; the electron and phonon temperatures are marked by the orange dotted line and dashed line, separately.

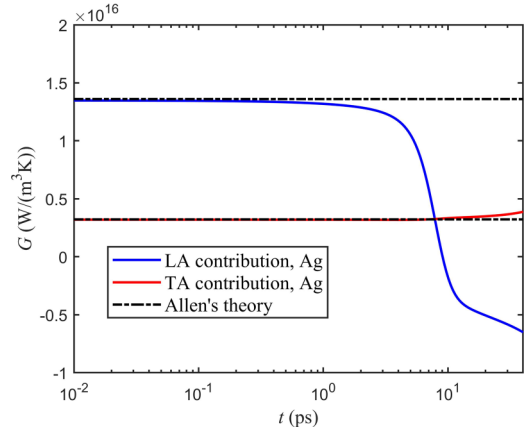


FIG. 3. The contribution from TA and LA branch to the  $e$ - $ph$  coupling constant for silver: the blue and red lines represent the result of the present model contributed by the LA and TA branches, respectively, whereas the dash-dot line denotes that of Allen's theory [34].

nonequilibrium between different phonon branches always exists. Finally, energy backflow occurs and the  $e$ - $ph$  coupling constant rapidly decreases. The present exploration of the time-dependent  $e$ - $ph$  coupling constant by our model is significant for the description of the electron and phonon coupling process in the femtosecond pump-probe experiments. The use of an invariable  $e$ - $ph$  coupling constant in the continuum TTM model requires further reexamination in the near future.

In addition, the different types of initial condition are investigated. First of all, the Gaussian-type initial distribution for electrons [34] can be straightforwardly incorporated, the influence of which on the  $e$ - $ph$  coupling constant compared to the currently preassumed high temperature condition is checked and shown in the Fig. 5(a). The Gaussian-type initial condition that approximately amounts to an effective electron temperature of 980 K has no effect on the result of the  $e$ - $ph$  coupling constant. Moreover, the influence by different values of preassumed electron temperature is also investigated in Fig. 5(b). The  $e$ - $ph$  coupling constant is nearly independent of electron temperature lower than 1000 K, which agrees with the conclusion in the *ab initio* calculation [30]. It clearly shows that the occurrence of the reduction of the  $e$ - $ph$  coupling constant is slightly influenced by the choice of different electron initial temperatures. This may arise from the temperature dependence of relaxation time. These results further validate the present model with more general application.

### B. Spatial nonequilibrium effect on $e$ - $ph$ coupling constant

In this section, the  $e$ - $ph$  coupling constant is calculated when the characteristic length of metals is reduced to nanoscale size. The quantum effect, which might be significant below nanometers, will not be considered in the present work as the first step. The cross-plane electron and phonon coupling transport through a thin gold film is simulated with the isothermal boundary and periodic boundary condition exerted on the  $x$  direction and the  $y$  direction, respectively. The  $z$  direction is omitted for simplicity. The temperature of  $T_h = 310$  K and  $T_c = 290$  K is assigned on the electron and

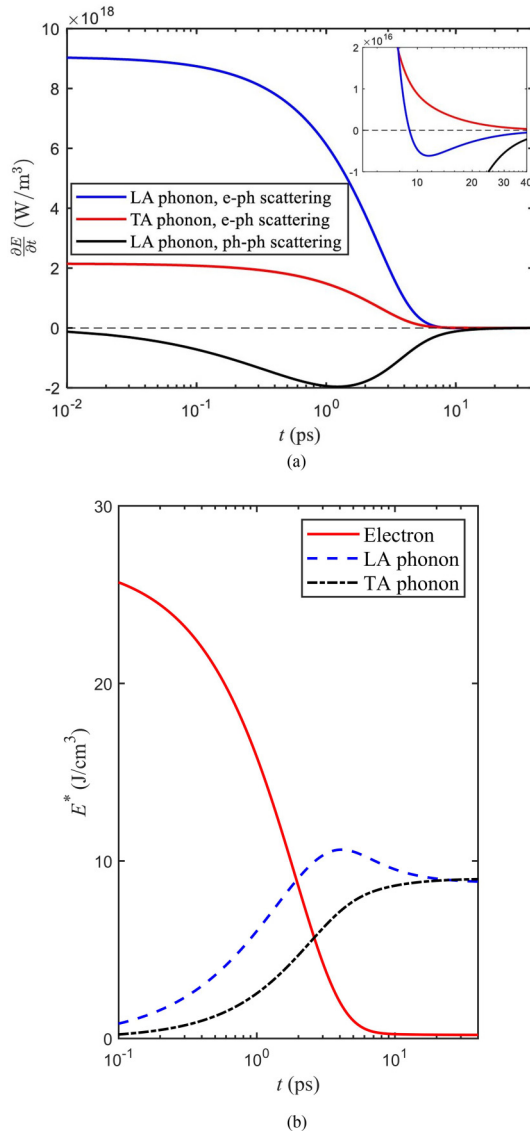


FIG. 4. Time-dependent phonon energy density change rate and the excess energy density of electron and phonon for silver: (a) phonon energy density change rate; the blue and black solid lines represent the result of the LA phonon by  $e$ - $ph$  scattering and  $ph$ - $ph$  scattering, separately, whereas the red line denotes that of the TA phonon by  $e$ - $ph$  scattering, and the dashed line is shown for eye guidance; the energy density change rate of the TA phonon by  $ph$ - $ph$  scattering is correspondingly inverse with that of the LA phonon due to the energy conservation principle during the  $ph$ - $ph$  scattering process; the inset is the magnified figure of the period from 5 to 40 ps. (b) The excess energy density of electron and phonon; the red line represents the result of electron whereas the blue dashed and black dash-dot lines denote that of the LA phonon and TA phonon, respectively.

phonon simultaneously at the left-hand and right-hand sides of the  $x$  direction, respectively. The thicknesses of 400, 80, and 5 nm are, respectively, simulated with a width of 2 nm for the lateral periodic boundary. In numerical solution, the number of abscissas of the GL quadrature is chosen as 48 and 48 points for electron energy and phonon spectrum, respectively, and 32 points for both the discretization of azimuth and polar

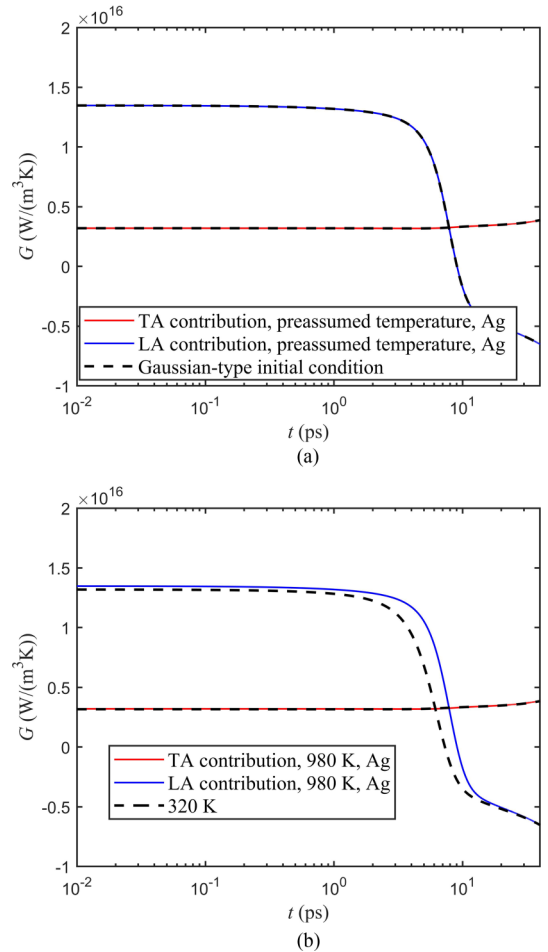


FIG. 5. The influence of different types of electron initial condition on the  $e$ - $ph$  coupling constant for silver: (a) Gaussian-type initial state vs the preassumed high-temperature condition; the blue and red lines represent the results of the preassumed temperature condition whereas the black dashed line denotes that of the Gaussian-type initial state. (b) The different values of preassumed initial electron temperature; the blue and red lines represent the results of the initial electron temperature of 980 K whereas the black dashed line denotes that of initial electron temperature of 320 K.

angle. The number of spatial grids is 201, 81, and 41 for thicknesses of 400, 80, and 5 nm, separately, with three nodes for the  $y$  direction. Therefore, the  $e$ - $ph$  coupling constant in Eq. (32) is shown in Fig. 6. Meanwhile, the local electron and phonon temperatures calculated by Eqs. (33) and (34) are further normalized as  $\Theta = (T - T_c)/(T_h - T_c)$  and displayed. When the temperatures of electrons and phonons gradually coincide as clearly shown in the middle region in Figs. 6(a) and 6(b), the amount of energy exchange between electrons and phonons tends to be zero. The use of expression (32) to calculate the  $e$ - $ph$  coupling constant is meaningless and thus the result of the  $e$ - $ph$  coupling constant is not displayed in this middle region.

The mean free path (MFP) of phonons is about one order of magnitude smaller than that of electrons in metals [20]. Thus, it is more difficult for electrons in the thin film to be sufficiently thermalized with the isothermal boundaries. It is

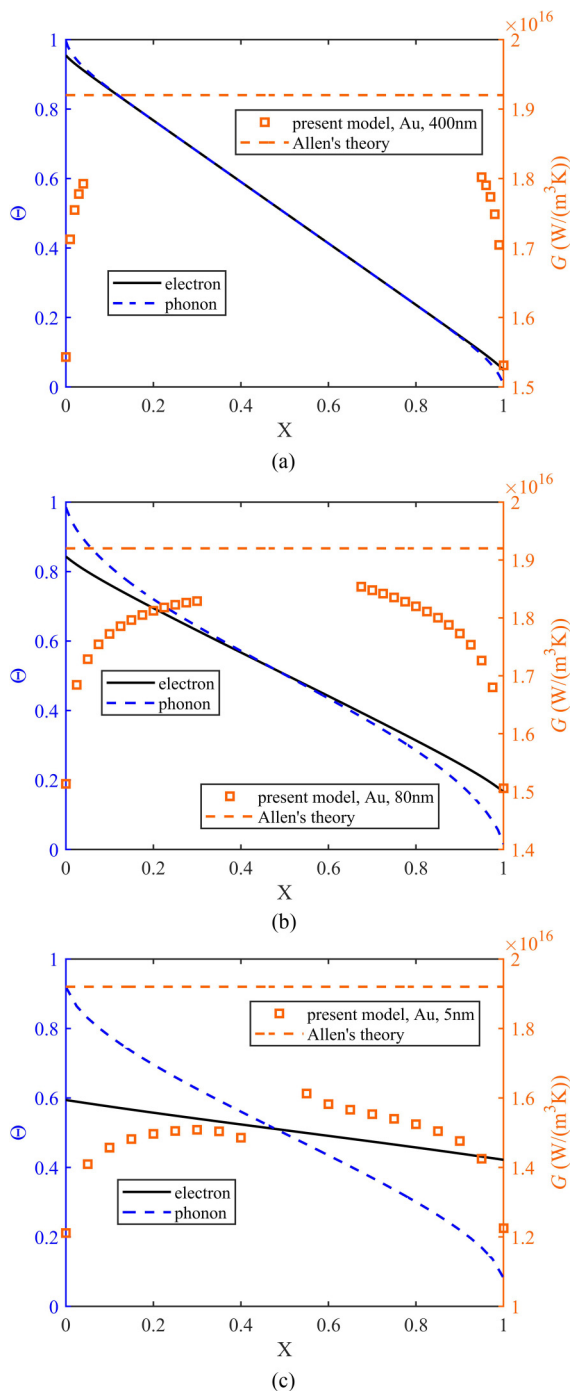


FIG. 6. The  $e$ - $ph$  coupling constant and the nondimensional temperature  $\Theta = (T - T_c)/(T_h - T_c)$  of electrons and phonons for the thin gold film of different thicknesses: (a) 400 nm; (b) 80 nm; (c) 5 nm. The hollow squares represent the  $e$ - $ph$  coupling constant calculated by the present model whereas the orange dashed line denotes that from Allen's theory [34]; the nondimensional electron and phonon temperature are marked by the black solid line and blue dashed line, respectively.

manifested by a larger temperature jump of electrons than that of phonons at the boundary, which further increases as the film thickness decreases. Consequently, nonequilibrium between

electrons and phonons exists, and then an energy exchange occurs. However, the energy exchange (shown in the  $e$ - $ph$  coupling constant) is weakened compared to Allen's theoretical calculation, which shall be attributed to the spatial nonequilibrium effect of electrons. In other words, electrons are more likely to reach the boundary before they exchange energy with phonons so that the  $e$ - $ph$  coupling constant decreases near the boundary. In addition, the  $e$ - $ph$  coupling constant further decreases by the increase of this spatial nonequilibrium effect as the film thickness decreases. The other metals including aluminum, silver, and copper exhibit similar results not shown here. This exploration will promote the fundamental understanding of electron and phonon coupling at very small scale. Generally, the nonequilibrium effects of electrons and phonons are increasingly important at nanoscale. As a result, the electron drag and phonon drag might play a non-negligible role at this small scale besides at low temperature. It has been rarely touched upon in the literature and requires more studies in the near future.

#### IV. CONCLUSIONS

In the present work, an electron-phonon ( $e$ - $ph$ ) coupling model is proposed through transforming the original  $e$ - $ph$  and  $ph$ - $e$  scattering terms in the coupled electron and phonon Boltzmann transport equations into the relaxation time approximation forms. This model is applied to investigate the  $e$ - $ph$  coupling constant when the temporal or spatial nonequilibrium effects are important. We demonstrate a verification of the coupling model by numerical modeling of the ultrafast dynamics process in femtosecond pump-probe experiments, which shows generally consistent results with the full integral treatment of scattering terms. The  $e$ - $ph$  coupling constant decreases rapidly due to the temporal nonequilibrium effect between different phonon branches. Moreover, the  $e$ - $ph$  coupling constant is much reduced by the nonequilibrium of electrons in confined space. As the nonequilibrium effect is intrinsically included, this  $e$ - $ph$  coupling model provides a feasible tool for the theoretical description of coupled electron and phonon transport systems at micro- and nanoscale. The present work will promote the fundamental understanding and modeling of the electron and phonon coupling process.

#### ACKNOWLEDGMENTS

This work is financially supported by NSF of China (Grant No. U1837602). Our simulations are run on the "Explorer 100" cluster of Tsinghua National Laboratory for Information Science and Technology. The authors appreciate helpful discussions with Y. Y. Guo and G. Yang.

#### APPENDIX A: DETERMINATION OF PSEUDOTEMPERATURES

We consider the zero-order moment equations through multiplying Eqs. (24) and (20) by  $|\epsilon_{\mathbf{k}} - \mu|$  and  $\hbar\omega_{\mathbf{Q},p}$ ,

respectively, and summing over the wave vector space:

$$\sum_{\mathbf{k}} |\varepsilon_{\mathbf{k}} - \mu| \frac{\partial \mathbf{g}_{\mathbf{k}}}{\partial t} + \sum_{\mathbf{k}} \mathbf{v}_e |\varepsilon_{\mathbf{k}} - \mu| \cdot \nabla_{\mathbf{r}} \mathbf{g}_{\mathbf{k}} = \sum_{\mathbf{k}} -|\varepsilon_{\mathbf{k}} - \mu| \frac{\mathbf{g}_{\mathbf{k}} - \mathbf{g}_{\mathbf{k}}^{eq}(\tilde{T}_e)}{\tau_{e-ph}(\varepsilon)}, \quad (\text{A1})$$

$$\sum_{\mathbf{Q},p} \hbar \omega_{\mathbf{Q},p} \frac{\partial n_{\mathbf{Q},p}}{\partial t} + \sum_{\mathbf{Q},p} \mathbf{v}_{ph,p} \hbar \omega_{\mathbf{Q},p} \cdot \nabla_{\mathbf{r}} n_{\mathbf{Q},p} = \sum_{\mathbf{Q},p} -\hbar \omega_{\mathbf{Q},p} \frac{n_{\mathbf{Q},p} - n_{\mathbf{Q},p}^{eq}(\tilde{T}_e)}{\tau_{ph-e}(\omega, p)} + \sum_{\mathbf{Q},p} -\hbar \omega_{\mathbf{Q},p} \frac{n_{\mathbf{Q},p} - n_{\mathbf{Q},p}^{eq}(\tilde{T}_{ph})}{\tau_{U,ph-ph}}. \quad (\text{A2})$$

Moreover, the energy balance equations require

$$\frac{\partial E_e}{\partial t} + \nabla \cdot \mathbf{q}_e = -\Psi_{e-ph}, \quad (\text{A3})$$

$$\frac{\partial E_{ph}}{\partial t} + \nabla \cdot \mathbf{q}_{ph} = \Psi_{e-ph}, \quad (\text{A4})$$

where  $\Psi_{e-ph}$  denotes the energy transfer from electrons to phonons. The heat flux of electrons and phonons is defined as  $\mathbf{q}_e = \sum_{\mathbf{k}} \mathbf{v}_e |\varepsilon_{\mathbf{k}} - \mu| \mathbf{g}_{\mathbf{k}}$ ,  $\mathbf{q}_{ph} = \sum_{\mathbf{Q},p} \mathbf{v}_{ph,p} \hbar \omega_{\mathbf{Q},p} n_{\mathbf{Q},p}$ , separately. Correspondingly, comparing the energy balance equations with the zero-order moment equations, it generally gives the equations:

$$\sum_{\mathbf{k}} -|\varepsilon_{\mathbf{k}} - \mu| \frac{\mathbf{g}_{\mathbf{k}} - \mathbf{g}_{\mathbf{k}}^{eq}(\tilde{T}_e)}{\tau_{e-ph}(\varepsilon)} + \sum_{\mathbf{Q},p} -\hbar \omega_{\mathbf{Q},p} \frac{n_{\mathbf{Q},p} - n_{\mathbf{Q},p}^{eq}(\tilde{T}_e)}{\tau_{ph-e}(\omega, p)} = 0, \quad (\text{A5})$$

$$\sum_{\mathbf{Q},p} -\hbar \omega_{\mathbf{Q},p} \frac{n_{\mathbf{Q},p} - n_{\mathbf{Q},p}^{eq}(\tilde{T}_{ph})}{\tau_{U,ph-ph}} = 0, \quad (\text{A6})$$

which are actually (26) and (25) in the main text. In other words, Eqs. (A5) and (A6) describe the energy conservation principle during the  $e-ph$  and  $ph-ph$  scattering processes, respectively. Thus, these two equations are implemented to calculate the electron and phonon pseudotemperatures.

## APPENDIX B: DOM SCHEME

A transient two-dimensional scheme is considered whereas the extension to three-dimensional (3D) problem is straightforward. For a short abbreviation,  $I$  and  $\phi$  are used to denote  $I_{\varepsilon}$  and  $\phi_{\omega,p}$ , separately. Considering the discretization of the angular and frequency/energy domains by the abscissas of the Gauss-Legendre (GL) quadrature, the intensity forms of electron and phonon BTEs (28) and (29) reduce to

$$\frac{\partial I_n^{\theta,\varphi}}{v_{e,n} \partial t} + u_{\theta} \frac{\partial I_n^{\theta,\varphi}}{\partial x} + \eta_{\theta}^{\varphi} \frac{\partial I_n^{\theta,\varphi}}{\partial y} = -\frac{I_n^{\theta,\varphi} - I_n^{eq}(\tilde{T}_e)}{(v_e \tau_{e-ph})_n}, \quad (\text{B1})$$

$$\frac{\partial \phi_{m_p}^{\theta,\varphi}}{v_{ph,m_p} \partial t} + u_{\theta} \frac{\partial \phi_{m_p}^{\theta,\varphi}}{\partial x} + \eta_{\theta}^{\varphi} \frac{\partial \phi_{m_p}^{\theta,\varphi}}{\partial y} = -\frac{\phi_{m_p}^{\theta,\varphi} - \phi_{m_p}^{eq}(\tilde{T}_e)}{(v_{ph} \tau_{ph-e})_{m_p}} - \frac{\phi_{m_p}^{\theta,\varphi} - \phi_{m_p}^{eq}(\tilde{T}_{ph})}{(v_{ph} \tau_{U,ph-ph})_{m_p}}, \quad (\text{B2})$$

where  $n = 1, 2, \dots, N_e$  and  $m_p = 1, 2, \dots, N_{ph,p}$  are the discrete electron energy nodes and spectral nodes of phonon polarization  $p$ , respectively.  $v_{e,n}$  and  $v_{ph,m_p}$  are the module of electron drift velocity and phonon group velocity of different branches.  $\theta = 1, 2, \dots, N_{\theta}$  and  $\varphi = 1, 2, \dots, N_{\varphi}$  are the discrete nodes for the polar angle  $[0, \pi]$  and semi azimuth angle  $[0, \pi]$ , separately, with  $\eta_{\theta}^{\varphi} = \sqrt{1 - u_{\theta}^2} \cos[(1 + u_{\varphi})\pi/2]$ ,  $u_{\theta}$  and  $u_{\varphi}$  being the corresponding abscissas of GL quadrature.

Subsequently, the implicit and first-order upwind scheme is applied to the temporal and spatial discretization. Considering the signs of  $u_{\theta}$  and  $\eta_{\theta}^{\varphi}$ , the Eqs. (B1) and (B2) are further written into the discrete forms by the general format

$$\frac{I_{n,i,j}^{\theta,\varphi,t+1} - I_{n,i,j}^{\theta,\varphi,t}}{v_{e,n} \Delta t} + \frac{u_{\theta} + |u_{\theta}|}{2} \frac{I_{n,i,j}^{\theta,\varphi,t+1} - I_{n,i-1,j}^{\theta,\varphi,t+1}}{\Delta x} + \frac{u_{\theta} - |u_{\theta}|}{2} \frac{I_{n,i+1,j}^{\theta,\varphi,t+1} - I_{n,i,j}^{\theta,\varphi,t+1}}{\Delta x} + \frac{\eta_{\theta}^{\varphi} + |\eta_{\theta}^{\varphi}|}{2} \frac{I_{n,i,j}^{\theta,\varphi,t+1} - I_{n,i,j-1}^{\theta,\varphi,t+1}}{\Delta y} + \frac{\eta_{\theta}^{\varphi} - |\eta_{\theta}^{\varphi}|}{2} \frac{I_{n,i,j+1}^{\theta,\varphi,t+1} - I_{n,i,j}^{\theta,\varphi,t+1}}{\Delta y} = -\frac{I_{n,i,j}^{\theta,\varphi,t+1} - I_{n,i,j}^{eq,t+1}(\tilde{T}_e)}{(v_e \tau_{e-ph})_n}, \quad (\text{B3})$$

$$\frac{\phi_{m_p,i,j}^{\theta,\varphi,t+1} - \phi_{m_p,i,j}^{\theta,\varphi,t}}{v_{ph,m_p} \Delta t} + \frac{u_{\theta} + |u_{\theta}|}{2} \frac{\phi_{m_p,i,j}^{\theta,\varphi,t+1} - \phi_{m_p,i-1,j}^{\theta,\varphi,t+1}}{\Delta x} + \frac{u_{\theta} - |u_{\theta}|}{2} \frac{\phi_{m_p,i+1,j}^{\theta,\varphi,t+1} - \phi_{m_p,i,j}^{\theta,\varphi,t+1}}{\Delta x} + \frac{\eta_{\theta}^{\varphi} + |\eta_{\theta}^{\varphi}|}{2} \frac{\phi_{m_p,i,j}^{\theta,\varphi,t+1} - \phi_{m_p,i,j-1}^{\theta,\varphi,t+1}}{\Delta y} + \frac{\eta_{\theta}^{\varphi} - |\eta_{\theta}^{\varphi}|}{2} \frac{\phi_{m_p,i,j+1}^{\theta,\varphi,t+1} - \phi_{m_p,i,j}^{\theta,\varphi,t+1}}{\Delta y} = -\frac{\phi_{m_p,i,j}^{\theta,\varphi,t+1} - \phi_{m_p,i,j}^{eq,t+1}(\tilde{T}_e)}{(v_{ph} \tau_{ph-e})_{m_p}} - \frac{\phi_{m_p,i,j}^{\theta,\varphi,t+1} - \phi_{m_p,i,j}^{eq,t+1}(\tilde{T}_{ph})}{(v_{ph} \tau_{U,ph-ph})_{m_p}}. \quad (\text{B4})$$

In Eqs. (B3) and (B4),  $i = 1, 2, \dots, N_x$  and  $j = 1, 2, \dots, N_y$  denote the spatial notes in the  $x$  direction and  $y$  direction, respectively, whereas  $t = 0, 1, 2, \dots, N_t$  represents the temporal nodes. Thus, the discrete electron and phonon intensities are derived from Eqs. (B3) and (B4), separately:

$$I_{n,i,j}^{\theta,\varphi,t+1} = \frac{I_{n,i,j}^{\theta,\varphi,t} + \alpha_{e-ph} I_{n,i,j}^{eq,t+1}(\tilde{T}_e) + \frac{c_n^u + |c_n^u|}{2} I_{n,i-1,j}^{\theta,\varphi,t+1} + \frac{|c_n^u| - c_n^u}{2} I_{n,i+1,j}^{\theta,\varphi,t+1} + \frac{c_n^\eta + |c_n^\eta|}{2} I_{n,i,j-1}^{\theta,\varphi,t+1} + \frac{|c_n^\eta| - c_n^\eta}{2} I_{n,i,j+1}^{\theta,\varphi,t+1}}{1 + \alpha_{e-ph} + |c_n^u| + |c_n^\eta|}, \quad (\text{B5})$$

$$\phi_{m_p,i,j}^{\theta,\varphi,t+1} = \frac{\phi_{m_p,i,j}^{\theta,\varphi,t} + \Phi_{m_p,i,j}^{eq,t+1} + \frac{c_{m_p}^u + |c_{m_p}^u|}{2} \phi_{m_p,i-1,j}^{\theta,\varphi,t+1} + \frac{|c_{m_p}^u| - c_{m_p}^u}{2} \phi_{m_p,i+1,j}^{\theta,\varphi,t+1} + \frac{c_{m_p}^\eta + |c_{m_p}^\eta|}{2} \phi_{m_p,i,j-1}^{\theta,\varphi,t+1} + \frac{|c_{m_p}^\eta| - c_{m_p}^\eta}{2} \phi_{m_p,i,j+1}^{\theta,\varphi,t+1}}{1 + \alpha_{ph-e} + \alpha_{ph-ph} + |c_{m_p}^u| + |c_{m_p}^\eta|}, \quad (\text{B6})$$

with

$$c_n^u = v_{e,n} u_\theta \Delta t / \Delta x, \quad c_n^\eta = v_{e,n} \eta_\theta^\varphi \Delta t / \Delta y, \quad c_{m_p}^u = v_{ph,m_p} u_\theta \Delta t / \Delta x, \quad c_{m_p}^\eta = v_{ph,m_p} \eta_\theta^\varphi \Delta t / \Delta y,$$

$$\alpha_{e-ph} = \Delta t / \tau_{e-ph,n}, \quad \alpha_{ph-e} = \Delta t / \tau_{ph-e,m_p}, \quad \alpha_{ph-ph} = \Delta t / \tau_{U,ph-ph,m_p}, \quad \Phi_{m_p,i,j}^{eq,t+1} = \alpha_{ph-e} \phi_{m_p,i,j}^{eq,t+1}(\tilde{T}_e) + \alpha_{ph-ph} \phi_{m_p,i,j}^{eq,t+1}(\tilde{T}_{ph}). \quad (\text{B7})$$

The pseudotemperatures of phonons and electrons are thus calculated based on the numerical solution of Eqs. (30) and (31) by dichotomy or Newton's method:

$$4\pi \sum_p \frac{\omega_{\max,p}}{2} \sum_{m_p=1}^{N_{ph,p}} \frac{\phi_{m_p}^{eq}(\tilde{T}_{ph,i,j}^{t+1})}{(v_{ph} \tau_{U,ph-ph})_{m_p}} w_{m_p} = \pi \sum_p \frac{\omega_{\max,p}}{2} \sum_{m_p=1}^{N_{ph,p}} \sum_{\theta=1}^{N_\theta} \sum_{\varphi=1}^{N_\varphi} \frac{\phi_{m_p,i,j}^{\theta,\varphi,t+1}}{(v_{ph} \tau_{U,ph-ph})_{m_p}} w_\varphi w_\theta w_{m_p}, \quad (\text{B8})$$

$$4\pi \varepsilon_{\text{HFW}} \sum_{n=1}^{N_e} \frac{I_n^{eq}(\tilde{T}_{e,i,j}^{t+1})}{(v_e \tau_{e-ph})_n} w_n + 4\pi \sum_p \frac{\omega_{\max,p}}{2} \sum_{m_p=1}^{N_{ph,p}} \frac{\phi_{m_p}^{eq}(\tilde{T}_{e,i,j}^{t+1})}{(v_{ph} \tau_{ph-e})_{m_p}} w_{m_p} \\ = \pi \varepsilon_{\text{HFW}} \sum_{n=1}^{N_e} \sum_{\theta=1}^{N_\theta} \sum_{\varphi=1}^{N_\varphi} \frac{I_{n,i,j}^{\theta,\varphi,t+1}}{(v_e \tau_{e-ph})_n} w_\varphi w_\theta w_n + \pi \sum_p \frac{\omega_{\max,p}}{2} \sum_{m_p=1}^{N_{ph,p}} \sum_{\theta=1}^{N_\theta} \sum_{\varphi=1}^{N_\varphi} \frac{\phi_{m_p,i,j}^{\theta,\varphi,t+1}}{(v_{ph} \tau_{ph-e})_{m_p}} w_\varphi w_\theta w_{m_p}, \quad (\text{B9})$$

where  $w_\varphi$ ,  $w_\theta$ ,  $w_n$ , and  $w_{m_p}$  are the corresponding weight coefficients with  $\varepsilon_{\text{HFW}}$  the half-width of the Fermi window. Similarly, the macroscopic variables including local electron, phonon temperature and  $e$ - $ph$  coupling constant are computed based on formulas (32)–(34):

$$4\pi \varepsilon_{\text{HFW}} \sum_{n=1}^{N_e} \frac{I_n^{eq}(T_{e,i,j}^{t+1})}{v_{e,n}} w_n = \pi \varepsilon_{\text{HFW}} \sum_{n=1}^{N_e} \sum_{\theta=1}^{N_\theta} \sum_{\varphi=1}^{N_\varphi} \frac{I_{n,i,j}^{\theta,\varphi,t+1}}{v_{e,n}} w_\varphi w_\theta w_n, \quad (\text{B10})$$

$$4\pi \sum_p \frac{\omega_{\max,p}}{2} \sum_{m_p=1}^{N_{ph,p}} \frac{\phi_{m_p}^{eq}(T_{ph,i,j}^{t+1})}{v_{ph,m_p}} w_{m_p} = \pi \sum_p \frac{\omega_{\max,p}}{2} \sum_{m_p=1}^{N_{ph,p}} \sum_{\theta=1}^{N_\theta} \sum_{\varphi=1}^{N_\varphi} \frac{\phi_{m_p,i,j}^{\theta,\varphi,t+1}}{v_{ph,m_p}} w_\varphi w_\theta w_{m_p}, \quad (\text{B11})$$

$$G_{i,j}^{t+1} = \frac{4\pi \sum_p \frac{\omega_{\max,p}}{2} \sum_{m_p=1}^{N_{ph,p}} \frac{\phi_{m_p}^{eq}(\tilde{T}_{e,i,j}^{t+1})}{(v_{ph} \tau_{ph-e})_{m_p}} w_{m_p} - \pi \sum_p \frac{\omega_{\max,p}}{2} \sum_{m_p=1}^{N_{ph,p}} \sum_{\theta=1}^{N_\theta} \sum_{\varphi=1}^{N_\varphi} \frac{\phi_{m_p,i,j}^{\theta,\varphi,t+1}}{(v_{ph} \tau_{ph-e})_{m_p}} w_\varphi w_\theta w_{m_p}}{\tilde{T}_{e,i,j}^{t+1} - \tilde{T}_{ph,i,j}^{t+1}}. \quad (\text{B12})$$

In addition, the isothermal boundary for the  $x$  direction and periodic boundary for the  $y$  direction are shown, respectively:

$$I_{n,x=0,j}^{u_\theta > 0, \varphi, t+1} = I_n^{eq}(T_h), \quad I_{n,x=L,j}^{u_\theta < 0, \varphi, t+1} = I_n^{eq}(T_c), \quad \phi_{m_p,x=0,j}^{u_\theta > 0, \varphi, t+1} = \phi_{m_p}^{eq}(T_h), \quad \phi_{m_p,x=L,j}^{u_\theta < 0, \varphi, t+1} = \phi_{m_p}^{eq}(T_c), \quad (\text{B13})$$

$$I_{n,i,y=0}^{\theta, \eta_\theta^\varphi > 0, t+1} = I_{n,i,y=H}^{\theta, \eta_\theta^\varphi > 0, t+1}, \quad I_{n,i,y=H}^{\theta, \eta_\theta^\varphi < 0, t+1} = I_{n,i,y=0}^{\theta, \eta_\theta^\varphi < 0, t+1}, \quad \phi_{m_p,i,y=0}^{\theta, \eta_\theta^\varphi > 0, t+1} = \phi_{m_p,i,y=H}^{\theta, \eta_\theta^\varphi > 0, t+1}, \quad \phi_{m_p,i,y=H}^{\theta, \eta_\theta^\varphi < 0, t+1} = \phi_{m_p,i,y=0}^{\theta, \eta_\theta^\varphi < 0, t+1}, \quad (\text{B14})$$

whereas other types of boundaries can be directly referred from our previous work [40].

Therefore, the computational procedures of the DOM scheme for the coupled electron and phonon BTEs is as follows:

(a) Initialize the electron and phonon intensity, and pseudoequilibrium intensity field at the moment  $t + 1$  by that of the last time step.

(b) Implement the boundary conditions.

(c) Update the electron and phonon intensity field by Eqs. (B5) and (B6).

(d) Calculate the electron and phonon pseudotemperatures based on Eqs. (B8) and (B9), and the corresponding pseudoequilibrium intensity.

(e) Compare the pseudoequilibrium intensity with that of the last iteration; if the convergence criterion is not satisfied, go back to step (b) until it is satisfied.

(f) Compute the macroscopic variables and then go to the next time step and loop from step (a) until finishing the prescribed time steps or reaching the steady state.

- [1] G. Eesley, Observation of Nonequilibrium Electron Heating in Copper, *Phys. Rev. Lett.* **51**, 2140 (1983).
- [2] B. Rethfeld, A. Kaiser, M. Vicanek, and G. Simon, Ultrafast dynamics of nonequilibrium electrons in metals under femtosecond laser irradiation, *Phys. Rev. B* **65**, 214303 (2002).
- [3] S. D. Brorson, J. G. Fujimoto, and E. P. Ippen, Femtosecond Electronic Heat-Transport Dynamics in Thin Gold Films, *Phys. Rev. Lett.* **59**, 1962 (1987).
- [4] H. Elsayed-Ali, T. Norris, M. Pessot, and G. Mourou, Time-Resolved Observation of Electron-Phonon Relaxation in Copper, *Phys. Rev. Lett.* **58**, 1212 (1987).
- [5] W. S. Fann, R. Storz, H. W. K. Tom, and J. Bokor, Electron thermalization in gold, *Phys. Rev. B* **46**, 13592 (1992).
- [6] W. Fann, R. Storz, H. Tom, and J. Bokor, Direct Measurement of Nonequilibrium Electron-Energy Distributions in Subpicosecond Laser-Heated Gold Films, *Phys. Rev. Lett.* **68**, 2834 (1992).
- [7] R. H. Groeneveld, R. Sprik, and A. Lagendijk, Effect of a nonthermal electron distribution on the electron-phonon energy relaxation process in noble metals, *Phys. Rev. B* **45**, 5079 (1992).
- [8] R. H. Groeneveld, R. Sprik, and A. Lagendijk, Femtosecond spectroscopy of electron-electron and electron-phonon energy relaxation in Ag and Au, *Phys. Rev. B* **51**, 11433 (1995).
- [9] V. Baranov and V. Kabanov, Theory of electronic relaxation in a metal excited by an ultrashort optical pump, *Phys. Rev. B* **89**, 125102 (2014).
- [10] L. Waldecker, R. Bertoni, R. Ernstorfer, and J. Vorberger, Electron-Phonon Coupling and Energy Flow in a Simple Metal Beyond the Two-Temperature Approximation, *Phys. Rev. X* **6**, 021003 (2016).
- [11] S. Ono, Nonequilibrium phonon dynamics beyond the quasiequilibrium approach, *Phys. Rev. B* **96**, 024301 (2017).
- [12] M. Obergfell and J. Demsar, Tracking the Time Evolution of the Electron Distribution Function in Copper by Femtosecond Broadband Optical Spectroscopy, *Phys. Rev. Lett.* **124**, 037401 (2020).
- [13] G. Chen, *Nanoscale Energy Transport and Conversion: A Parallel Treatment of Electrons, Molecules, Phonons, and Photons* (Oxford University Press, New York, 2005).
- [14] Y. Guo and M. Wang, Phonon hydrodynamics and its applications in nanoscale heat transport, *Phys. Rep.* **595**, 1 (2015).
- [15] S. Anisimov, B. Kapeliovich, and T. Perelman, Electron emission from metal surfaces exposed to ultrashort laser pulses, *Zh. Eksp. Teor. Fiz.* **66**, 776 (1974) [*Sov. Phys. JETP* **39**, 375 (1974)].
- [16] M. Kaganov, I. Lifshitz, and L. Tanatarov, Relaxation between electrons and the crystalline lattice, *Zh. Eksp. Teor. Fiz.* **31**, 232 (1957) [*Sov. Phys. JETP* **4**, 173 (1957)].
- [17] P. B. Allen, Theory of Thermal Relaxation of Electrons in Metals, *Phys. Rev. Lett.* **59**, 1460 (1987).
- [18] S. Brorson, A. Kazerooni, J. Moodera, D. Face, T. Cheng, E. Ippen, M. Dresselhaus, and G. Dresselhaus, Femtosecond Room-Temperature Measurement of the Electron-Phonon Coupling Constant  $\gamma$  in Metallic Superconductors, *Phys. Rev. Lett.* **64**, 2172 (1990).
- [19] M. Kaviani, *Heat Transfer Physics* (Cambridge University Press, New York, 2014).
- [20] T. M. Tritt, *Thermal Conductivity: Theory, Properties, and Applications* (Springer Science & Business Media, New York, 2005).
- [21] J. Hohlfeld, S.-S. Wellershoff, J. Güdde, U. Conrad, V. Jähnke, and E. Matthias, Electron and lattice dynamics following optical excitation of metals, *Chem. Phys.* **251**, 237 (2000).
- [22] J. H. Hodak, A. Henglein, and G. V. Hartland, Electron-phonon coupling dynamics in very small (between 2 and 8 nm diameter) Au nanoparticles, *J. Chem. Phys.* **112**, 5942 (2000).
- [23] H. E. Elsayed-Ali, T. Juhasz, G. O. Smith, and W. E. Bron, Femtosecond thermorefectivity and thermotransmissivity of polycrystalline and single-crystalline gold films, *Phys. Rev. B* **43**, 4488 (1991).
- [24] H. Orlande, M. Özisik, and D. Tzou, Inverse analysis for estimating the electron-phonon coupling factor in thin metal films, *J. Appl. Phys.* **78**, 1843 (1995).
- [25] A. Arbouet, C. Voisin, D. Christofilos, P. Langot, N. Del Fatti, F. Vallée, J. Lermé, G. Celep, E. Cottancin, M. Gaudry *et al.*, Electron-Phonon Scattering in Metal Clusters, *Phys. Rev. Lett.* **90**, 177401 (2003).
- [26] Y. P. Timalsina, X. Shen, G. Boruchowitz, Z. Fu, G. Qian, M. Yamaguchi, G.-C. Wang, K. M. Lewis, and T.-M. Lu, Evidence of enhanced electron-phonon coupling in ultrathin epitaxial copper films, *Appl. Phys. Lett.* **103**, 191602 (2013).
- [27] J. Hu, T. E. Karam, G. A. Blake, and A. H. Zewail, Ultrafast lattice dynamics of single crystal and polycrystalline gold nanofilms, *Chem. Phys. Lett.* **683**, 258 (2017).
- [28] T. Qiu and C. Tien, Size effects on nonequilibrium laser heating of metal films, *Trans. ASME* **115**, 842 (1993).
- [29] B. Mueller and B. Rethfeld, Relaxation dynamics in laser-excited metals under nonequilibrium conditions, *Phys. Rev. B* **87**, 035139 (2013).
- [30] Z. Lin, L. V. Zhigilei, and V. Celli, Electron-phonon coupling and electron heat capacity of metals under conditions of strong electron-phonon nonequilibrium, *Phys. Rev. B* **77**, 075133 (2008).
- [31] A. Jain and A. J. H. McGaughey, Thermal transport by phonons and electrons in aluminum, silver, and gold from first principles, *Phys. Rev. B* **93**, 081206(R) (2016).
- [32] Y. Wang, Z. Lu, and X. Ruan, First principles calculation of lattice thermal conductivity of metals considering phonon-phonon and phonon-electron scattering, *J. Appl. Phys.* **119**, 225109 (2016).
- [33] Z. Tong, S. Li, X. Ruan, and H. Bao, Comprehensive first-principles analysis of phonon thermal conductivity and electron-phonon coupling in different metals, *Phys. Rev. B* **100**, 144306 (2019).
- [34] S. Ono, Thermalization in simple metals: Role of electron-phonon and phonon-phonon scattering, *Phys. Rev. B* **97**, 054310 (2018).
- [35] J. K. Chen, D. Y. Tzou, and J. E. Beraun, A semiclassical two-temperature model for ultrafast laser heating, *Int. J. Heat Mass Transfer* **49**, 307 (2006).
- [36] A. K. Vallabhaneni, D. Singh, H. Bao, J. Murthy, and X. Ruan, Reliability of Raman measurements of thermal conductivity of single-layer graphene due to selective electron-phonon coupling: A first-principles study, *Phys. Rev. B* **93**, 125432 (2016).
- [37] P. Maldonado, K. Carva, M. Flammer, and P. M. Oppeneer, Theory of out-of-equilibrium ultrafast relaxation dynamics in metals, *Phys. Rev. B* **96**, 174439 (2017).

- [38] W. Miao, Y. Guo, X. Ran, and M. Wang, Deviation Monte Carlo scheme for thermal and electrical transport in metal nanostructures, *Phys. Rev. B* **99**, 205433 (2019).
- [39] J.-P. M. Péraud and N. G. Hadjiconstantinou, Efficient simulation of multidimensional phonon transport using energy-based variance-reduced Monte Carlo formulations, *Phys. Rev. B* **84**, 205331 (2011).
- [40] Y. Guo and M. Wang, Heat transport in two-dimensional materials by directly solving the phonon Boltzmann equation under Callaway's dual relaxation model, *Phys. Rev. B* **96**, 134312 (2017).
- [41] X. Ran and M. Wang, Efficiency improvement of discrete-ordinates method for interfacial phonon transport by Gauss-Legendre integral for frequency domain, *J. Comput. Phys.* **399**, 108920 (2019).
- [42] J. M. Ziman, *Electrons and Phonons: The Theory of Transport Phenomena in Solids* (The Clarendon Press, Oxford, 1960).
- [43] Y. G. Gurevich and O. Mashkevich, The electron-phonon drag and transport phenomena in semiconductors, *Phys. Rep.* **181**, 327 (1989).
- [44] N. H. Protik and D. A. Broido, Coupled transport of phonons and carriers in semiconductors: A case study of *n*-doped GaAs, *Phys. Rev. B* **101**, 075202 (2020).
- [45] M. Lundstrom, *Fundamentals of Carrier Transport* (Cambridge University Press, Cambridge, 2000).
- [46] G. A. Slack and S. Galginaitis, Thermal conductivity and phonon scattering by magnetic impurities in CdTe, *Phys. Rev.* **133**, A253 (1964).
- [47] Q. Hao, G. Chen, and M.-S. Jeng, Frequency-dependent Monte Carlo simulations of phonon transport in two-dimensional porous silicon with aligned pores, *J. Appl. Phys.* **106**, 114321 (2009).
- [48] Z. M. Zhang, *Nano/microscale Heat Transfer* (McGraw-Hill, New York, 2007).
- [49] C. Kittel, *Introduction to Solid State Physics* (John Wiley & Sons, Inc., New York, 2005).
- [50] A. Majumdar, Microscale heat conduction in dielectric thin films, *J. Heat Transfer* **115**, 7 (1993).
- [51] R. Stedman and G. Nilsson, Dispersion relations for phonons in aluminum at 80 and 300 °K, *Phys. Rev.* **145**, 492 (1966).
- [52] X. Ran, Y. Guo, and M. Wang, Interfacial phonon transport with frequency-dependent transmissivity by Monte Carlo simulation, *Int. J. Heat Mass Transfer* **123**, 616 (2018).
- [53] J. W. Lynn, H. G. Smith, and R. M. Nicklow, Lattice dynamics of gold, *Phys. Rev. B* **8**, 3493 (1973).
- [54] W. Kamitakahara and B. Brockhouse, Crystal dynamics of silver, *Phys. Lett. A* **29**, 639 (1969).
- [55] C. S. Jayanthi, E. Tosatti, and A. Fasolino, Self-consistent phonons, thermal properties, and vibrational instability of the copper crystal, *Phys. Rev. B* **31**, 470 (1985).
- [56] L. A. Girifalco and K. Kniaz, Anharmonicity in metals from the universal energy equation, *J. Mater. Res.* **12**, 311 (1997).
- [57] V. V. Kabanov and A. S. Alexandrov, Electron relaxation in metals: Theory and exact analytical solutions, *Phys. Rev. B* **78**, 174514 (2008).
- [58] G. Grimvall, *The Electron-Phonon Interaction in Metals* (North-Holland Publishing Co., New York, 1981).
- [59] J. L. Hostetler, A. N. Smith, D. M. Czajkowsky, and P. M. Norris, Measurement of the electron-phonon coupling factor dependence on film thickness and grain size in Au, Cr, and Al, *Appl. Opt.* **38**, 3614 (1999).
- [60] D. Gall, Electron mean free path in elemental metals, *J. Appl. Phys.* **119**, 085101 (2016).